NeuroImage 85 (2014) 6–27

Contents lists available at ScienceDirect

NeuroImage

journal homepage: www.elsevier.com/locate/ynimg

Review

A review on continuous wave functional near-infrared spectroscopy and imaging instrumentation and methodology

Felix Scholkmann [a], Stefan Kleiser [a], Andreas Jaakko Metz [a], Raphael Zimmermann [a,b], Juan Mata Pavia [a], Ursula Wolf [c], Martin Wolf [a,*]

[a] Biomedical Optics Research Laboratory, Division of Neonatology, University Hospital Zurich, 8091 Zurich, Switzerland
[b] Rehabilitation Engineering Laboratory, ETH Zürich, 8092 Zurich, Switzerland
[c] Institute of Complementary Medicine, University of Bern, 3010 Bern, Switzerland

ARTICLE INFO

Article history:
Accepted 3 May 2013
Available online 16 May 2013

Keywords:
Review
Near-infrared spectroscopy (NIRS)
Near-infrared imaging (NIRI)
Functional near-infrared spectroscopy (fNIRS)
Functional near-infrared imaging (fNIRI)
Continuous wave
Brain activity
Instrumentation

ABSTRACT

This year marks the 20th anniversary of functional near-infrared spectroscopy and imaging (fNIRS/fNIRI). As the vast majority of commercial instruments developed until now are based on continuous wave technology, the aim of this publication is to review the current state of instrumentation and methodology of continuous wave fNIRI. For this purpose we provide an overview of the commercially available instruments and address instrumental aspects such as light sources, detectors and sensor arrangements. Methodological aspects, algorithms to calculate the concentrations of oxy- and deoxyhemoglobin and approaches for data analysis are also reviewed.
From the single-location measurements of the early years, instrumentation has progressed to imaging initially in two dimensions (topography) and then three (tomography). The methods of analysis have also changed tremendously, from the simple modified Beer-Lambert law to sophisticated image reconstruction and data analysis methods used today. Due to these advances, fNIRI has become a modality that is widely used in neuroscience research and several manufacturers provide commercial instrumentation. It seems likely that fNIRI will become a clinical tool in the foreseeable future, which will enable diagnosis in single subjects.

Contents

* Corresponding author.
E-mail address: martin.wolf@usz.ch (M. Wolf).

1053-8119/$ – see front matter © 2013 Elsevier Inc. All rights reserved.
http://dx.doi.org/10.1016/j.neuroimage.2013.05.004

Introduction

Continuous light has been used to non-invasively investigate human tissue such as the breast, head and testes by transmitting the light through the body as early as at least in the 19th century (Bright, 1831; Curling, 1856; Cutler, 1929). More specifically, already in 1862 Hoppe-Seyler from Germany, described the spectrum of oxy-hemoglobin (O_2Hb) (Perutz, 1995) and in 1864 Stokes from the United Kingdom added the spectrum of deoxy-hemoglobin (HHb) and consequently discovered the importance of hemoglobin for the oxygen transport (Perutz, 1995). In 1876 von Vierordt, also from Germany, analyzed tissue by measuring the spectral changes of light penetrating tissue when the blood circulation was occluded (Severinghaus, 2007; von Vierordt, 1876) and in 1894 Hüfner from Germany spectroscopically determined absolute and relative amounts of O_2Hb and HHb in vitro (Hüfner, 1894). After decades of no relevant research in this field, in the 1930s the work on spectroscopic determination of tissue oxygenation was continued by several researchers. For example Nicolai, Germany, repeated the study of von Vierordt (Nicolai, 1932a,b), and Matthes and Gross, Germany, demonstrated for the first time the spectroscopic determination of O_2Hb and HHb in human tissue using two wavelengths, one in the red and near-infrared region (Matthes and Gross, 1938a,b,c).

In terms of quantification, an important first step was the discovery of the Beer–Lambert law first by the French mathematician Bouguer in 1729 (Bouguer, 1729). It is often attributed to the Swiss Lambert, although he cited Bouguers work in 1760 himself (Lambert, 1760). The law was extended by the German Beer to quantify concentrations in 1852 (Beer, 1852). Since the Beer–Lambert law is only valid in non-scattering media, it cannot be applied to biological tissue. Relatively recently therefore the modified Beer–Lambert law (MBLL) was developed by the British Delpy (Delpy et al., 1988), to take into account the light scattering. The MBLL is often used by many instruments described in this review. Further important steps were also analytical solutions of the diffusion equation (e.g. Arridge et al., 1992; Patterson et al., 1989) to quantitatively describe light transport in tissue.

Based on the insight of the relative transparency of the tissue including the skull in the near infrared range in 1977 Jobsis from the USA first demonstrated the feasibility to continuously and non-invasively monitor the concentration of O_2Hb and HHb ([O_2Hb] and [HHb]) in the brain (Jobsis, 1977). Therefore he is considered to be the initiator of near-infrared spectroscopy (NIRS).

His discovery led to designing and building of several NIRS instruments (Ferrari and Quaresima, 2012). All these instruments were continuous wave (CW) instruments. The term "continuous wave" means that the instrumentation is solely based on a light intensity measurement, i.e. near-infrared light is sent into the tissue and the intensity of the re-emerging (i.e. diffusely reflected) light is measured. This is in contrast to time resolved techniques such as time and frequency domain techniques, which, additionally to the intensity measurements also measure the time of flight, i.e. the time that the light needs to travel through the tissue. For a visualization of the three different techniques please refer to Fig. 1.

The disadvantage of CW systems is that they cannot fully determine the optical properties of tissue (i.e. light scattering (μ_s') and absorption (μ_a) coefficients) and therefore the [O_2Hb] and [HHb] cannot be determined absolutely. However, with a few reasonable assumptions it is possible to quantify changes in [O_2Hb] and [HHb]. Therefore, during the first years, NIRS instruments were mostly trend monitors, employed to study various physiological conditions and clinical interventions. Much research was aimed at obtaining absolute values either by physiological maneuvers (e.g. Edwards et al., 1988; Wyatt et al., 1990) or enhancing the instrumentation (e.g. Matcher et al., 1994, 1995b; Wolf et al., 1997). Later time resolved techniques were developed and became available and enabled to determine absolute values. This will not be discussed further, because it is not within the scope of this review.

1993 was a crucial year in the development of *functional* NIRS (fNIRS) of the brain. In the same year four research groups published results and demonstrated that it is possible to non-invasively investigate brain activity using fNIRS (Chance et al., 1993; Hoshi and Tamura, 1993; Kato et al., 1993; Villringer et al., 1993). Brain activity leads to an increase in oxygen consumption, which is accompanied by an increase in cerebral blood flow due to neurovascular coupling. This leads to a change in the local [O_2Hb] and [HHb] (Wolf et al., 2002), which can be detected non-invasively by fNIRS. These first measurements were carried out with simple instruments, which measured at one or a few locations. Since brain activity in response to a stimulation occurs only at specific locations in the brain, when measuring just at one location it is often difficult to find the correct position on the head

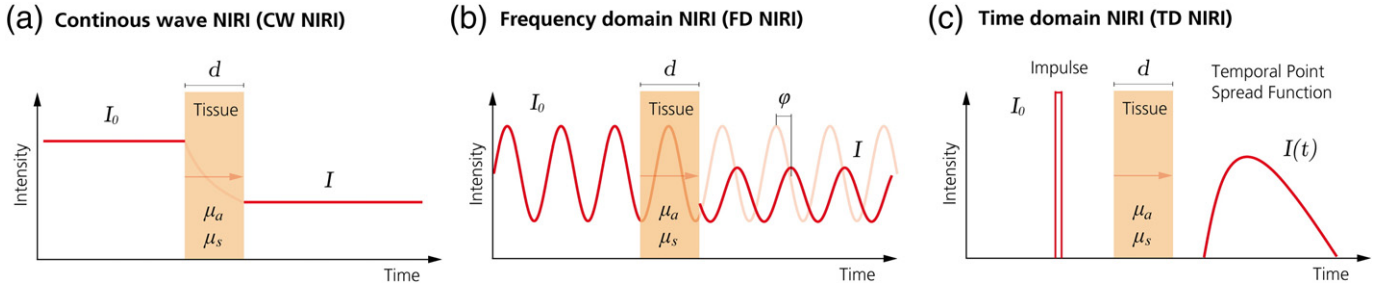

Fig. 1. Illustration of the three different NIRI techniques. The continuous wave technology emits light at a constant intensity and then only measures the changes in the intensity of the light that passed through the tissue. The frequency domain technology modulates the emitted light intensity and then measured the intensity of the detected light as well as the phase shift, which corresponds to the time of flight. The time domain technology emits an extremely short pulse of light into the tissue and measures the arrival times of the photons that emerge from the tissue. This technology yields the highest amount of information, but it is also the most complex technology. I_0: incident light signal, I: transmitted light signal, d: thickness of the medium, μ_a: absorption coefficient, μ_s: scattering coefficient, φ: phase delay, and $I(t)$: temporal point spread function of the transmitted light signal.

for the measurement. In addition, there is a scientific interest in measuring a spatial pattern, how the brain activity affects an area of the brain.

A next major step in the development was to design imaging instruments that covered a larger area of the head and enabled mapping of brain activity, i.e. to deliver *topographic* information (Ferrari and Quaresima, 2012; Maki et al., 1995). This had several advantages: it enabled to localize brain activity and the precise localization of the sensor was less important. This technology is called functional near infrared imaging (fNIRI). On the one hand, it was quite clear that it is highly important to expand the interrogated area by using imaging systems. On the other hand, quantification is not that important in neuroscience, i.e. it is more important to statistically significantly detect a change in brain activity than to quantify it in absolute terms. For these reasons up to today most imaging systems are based on CW technology. In addition, time resolved systems have a lower time resolution, are more expensive and the time of flight is generally a more noisy parameter than the intensity and therefore not useful for detecting small functional activations. In contrast, CW systems are relatively low cost, can be miniaturized and wireless systems and can be applied unobtrusively in everyday life situations or even freely moving animals (Muehlemann et al., 2008).

As a next step, sensor arrangements where several source detector distances are measured simultaneously, so-called overlapping measurements, enabled to apply *tomographic* approaches, i.e. image reconstructions in three dimensions (Joseph et al., 2006).

Today fNIRI has entered neuroscience as a research tool. It has been shown that fNIRI is reliable and trustworthy for research based on investigating groups of subjects, although reliability in single subjects is not sufficient yet (Kono et al., 2007; Plichta et al., 2006, 2007a,b; Schecklmann et al., 2008). Consequently, the number of publications on fNIRI in neuroscience has increased exponentially within the last years.

One of the next aims is to apply fNIRI clinically. For this purpose it will be compulsory to ensure a high reproducibility in single subjects. However, a sufficient reliability on the single subject level has not yet been achieved (Biallas et al., 2012a,b; Kono et al., 2007; Plichta et al., 2006, 2007a,b; Schecklmann et al., 2008). Hence, some research is currently focused on improving the reliability. Possible reasons for the lack in reliability are the superficial tissue (i.e. light has to penetrate several tissue layers such as e.g. skin and skull before it reaches the brain) or systemic physiological changes, which contaminate the signal of the brain and possibly instrumental shortcomings such as an insufficiency in spatial resolution and/or signal to noise ratio (SNR). Generally there are several possibilities to improve reliability: On the instrumental level, it is important to select appropriate wavelengths, light sources, detectors, and geometrical arrangements to avoid crosstalk and ensure a high SNR; on a methodological level the aim is to reduce the influence of superficial tissue or systemic components.

The aim of this paper is to review the current state of instrumentation and methodology of CW fNIRI. For this purpose we will give an overview of the commercially available instruments and address instrumental aspects such as light sources, detectors and sensor arrangements. Methodological aspects such as algorithms to determine [O_2Hb] and [HHb] and data analysis will also be reviewed.

There is a variety of terms used for NIRS. In general the term NIRS is often used as an overarching term for the whole technology, but in principle it only refers to NIRS systems measuring at single locations with up to four sensors, but without imaging capacity. Imaging systems, which we will call NIRI here, have more than 4 channels and produce two or three dimensional images. In the literature, 2D imaging systems are also called near infrared topography or mapping, or diffuse optical imaging. 3D imaging systems are also called near infrared tomography or mapping, or diffuse optical tomography or imaging. The term "diffuse" refers to the fact that due to the high μ_s' in tissue the propagation of photons through tissue can be modeled as a diffusion process. Unfortunately, the term "diffuse" is often misinterpreted as blurred or fuzzy, i.e. referring to a negative connotation of the technique, which clearly is not meant or adequate. As for magnetic resonance imaging (MRI), which was formerly referred to as nuclear magnetic resonance, the term "nuclear" falsely evoked the association of a radioactive method, we propose to abandon the term "diffuse" in the future to avoid this negative connotation. The spatially resolved measurement of brain activity in two and three dimensions we call *functional* NIRI (fNIRI). All systems (except for one) and methods reviewed here are generally about CW fNIRI and therefore the term "CW" will be omitted below.

Overview of commercially available imaging instrumentation

There is already a wide variety of commercially available fNIRI devices in the market. Therefore, researchers are likely to find devices suited for their respective needs. System complexity ranges from few sources and detectors suitable to image certain brain areas to systems covering the whole head. Some devices use sensor patches (D2, D3, D4, D7, D14, see Table 1) with integrated components whereas all others use optical fibers and flexible head-caps allowing for adjustments to the individual subject. Different systems offer different degrees of sensor comfort which is an important factor for studies with prolonged measurement times. While most fNIRI devices are larger in size and transportable on a cart, some can be attached to the subject and transmit data wirelessly to a control PC, offering new possibilities such as the analysis of gait or the unrestrained interaction of freely moving persons or animals. This variety of devices and concepts is also reflected in prices, which vary from some $10,000 for simple systems to several $100,000 for whole-head imaging systems.

Additionally to our pre-existing knowledge we have searched the internet for manufacturers of fNIRI devices. Subsequently we contacted all identified manufacturers of commercial fNIRI devices with a questionnaire and compiled an overview of devices with more than 4 channels in Table 1. All information presented has been retrieved from representatives of the corresponding manufacturer. Manufacturers often offer different set-ups for their devices and usually offer several accessory and software options. If this is the case, this variety is represented by spans of values. The URLs of all manufacturers were included to give the reader the possibility to contact manufacturers directly for more details.

The following properties apply to most or all devices and are not listed in Table 1:

- All devices except for device D7 are sold world-wide.
- All devices offer a software solution for computing hemoglobin changes from raw intensity data. Most devices measure relative changes in [O_2Hb] and [HHb] using the MBLL (Delpy et al., 1988). No information was obtained about the algorithms used in proprietary software of instruments D3, D4 and D13. We would like to emphasize, that unpublished algorithms are a considerable disadvantage in the scientific community, because they limit the possibility to interpret the results.
- For data evaluation, some manufacturers offer proprietary software, others make their software available and others prefer the use of open-source toolboxes such as HomER2 (Huppert et al., 2009; PMILab, 2012), NIRS-SPM, or NIRFAST (Dehghani et al., 2009a). The latter is more recommendable, because the algorithms are published/known and results can be interpreted accordingly. In addition, this allows for easier customization if desired. Such free post-processing tools can be used with most instruments.
- Instruments D1, D2 and D17 can optionally measure tissue oxygen saturation using spatially resolved spectroscopy (Challenges for classification and separation of the signal components section). This may also be possible with other devices by using proper optode arrangements, calibration and post-processing software.
- All devices can be exposed to ambient light without any risk of damaging the detectors. Although most devices remove smaller amounts of ambient light reaching the detectors either by hardware (devices

Table 1
Commercial NIRI devices: company websites can be found in the references. For the detailed description please refer to the text. Special comments: D2: has only 3 channels, but devices can easily be coupled (up to 8); D4: has only 4 channels, but devices can easily be coupled (up to 20); D5 + D6: have FDA approval, a previous version of these devices is presented in (Maki et al., 1995); D8: offers hair-penetrating optodes (Khan et al., 2012), device volume of 1 l + battery; D9–11: two systems can be paired for doubled emitters and detectors; D12: proximity detector embedded in each emitter; D13: two systems can be paired for doubled emitters and detectors, 7.5 Hz time-resolution using 8 Emitters; D14: can measure SpO_2, OEG-16 also available (no fast sampling, no SpO_2 measurement); D17: frequency domain instrument, otherwise comparable in functionality.

	Device	(Manufacturer), country	Time-res. [Hz]	#Emitter	#Detector	MUX	SDS [mm]	E-tech	Wavelengths [nm]	D-tech	Data	Wear	CE
D1	OXYMON MkIII[a]	(Artinis), Netherlands	250	32	16	t	a	Laser	760, 850*	APD	Raw	n	y
D2	PortaLite	(Artinis), Netherlands	50	3	1	t	20 + 25 / 30 + 35 + 40	LED	760, 850*	PD	Raw	y	y
D3	fNIR1100	(fNIR Devices), USA	2	1/1/4	2/4/10	t	20/25/25	LED	730, 850		Hb	n	n
D4	fNIR1100w	(fNIR Devices), USA	2	1	2/4	t	20/25	LED	730, 850		Hb	y	n
D5	ETG-4000	(Hitachi), Japan	10	18	8	f	20/30	Laser	695, 830	APD	Raw	n	y
D6	ETG-7100	(Hitachi), Japan	10	40	40	f	20/30	Laser	695, 830	APD	Raw	n	y
D7	WOT[b]	(Hitachi), Japan	5	8	8	t + f	30	Laser	705, 830	PD	Raw	y	n*
D8	Genie	(MRRA), USA	5.02	4 to16	8 to 32	c	a	LED	700, 830	PD	Raw	y	n
D9	NIRScout	(NIRx), USA	6.25 to 62.5	8 or 16	4 to 24	t + f	a	LED	760, 850	PD	Raw	n	y
D10	NIRScoutX	(NIRx), USA	6.25 to 62.5	48	32	t + f	a	LED	760, 850	PD	Raw	n	y
D11	NIRSport	(NIRx), USA	6.25 to 62.5	8	8	t + f	a	LED	760, 850	PD	Raw	y	y
D12	Brainsight NIRS	(Rogue Research), Canada	100	4 to16	8 to 32	f	a	Laser	685, 830, (808)*	APD	Raw	n	n*
D13	FOIRE-3000	(Shimadzu), Japan	7.5 to 40	4 to 16	4 to 16	t	a	Laser	780, 805, 830	PMT	OD	n	n
D14	OEG-SpO2	(Spectratech), Japan	1.52/12.2	6	6	c	30/25/15–40	LED	770, 840	PD	Raw	y*	n*
D15	CW6	(TechEn), USA	10 to 50	4 to 48	8 to 32	f	a	Laser	690, 830*	APD	Raw	n	y
D16	UCL Optical Topography System[c]	(University College London), UK	10 to 160	16	16	f	a	Laser	780, 850	APD	Raw	n	n
D17	Imagent	(ISS), USA	16 to 60	16 or 32	4 or 8	t	a	Laser	690, 830	PMT	Raw	n	y

[a] van der Sluijs et al. (1998).
[b] Atsumori et al. (2009).
[c] Everdell et al. (2005).

using frequency or code multiplexing and D1) or by software (instruments D2, D3 and D4), exposure to ambient light during measurements should be avoided, because the dynamic range of the detector will be decreased, additional shot noise will affect SNR negatively and high levels of ambient light may saturate the detectors, which completely invalidates the data.

- To reduce the running costs, all devices employ re-usable sensors that can be disinfected. A wide variety of optode holders or sensors are available for all devices, allowing also for measurements in children, except for D7 which is only intended for use in adults.
- Maximum averaged light emission per source is typically in the range of 5–20 mW optical power or below. Some devices (D2, D3, D4, D7, D14) use headprobes with integrated optical components. See also Light sources for fNIRI instruments section for more information on the types of light sources.
- NIRI devices are often characterized by their number of channels. If we define one channel as one path between one emitter including all its wavelengths and one detector, then the maximum (theoretical) number of channels for a 16 emitter and 32 detector system will be $16 * 32 = 512$ channels. Note that in practice detectors cannot detect light from very distant emitters (for example on the opposite side of an adult head) and that there may also be space constraints which may inhibit placing all optodes on the subject. Therefore, in practice the number of usable channels for such systems with 16 sources and 32 detectors is in the range of 50–200 channels and depends strongly on the optodes arrangement. Since this discrepancy might be misleading especially for large systems, no channel number is presented in Table 1.
- Some devices offer interfaces to allow for multi-modal imaging and have successfully been used for example in simultaneous measurements of fNIRI and MEG (Seki et al., 2012), EEG (Hebden et al., 2012; Leamy and Ward, 2010), fMRI (Habermehl et al., 2012a; Toronov et al., 2001; X. Zhang et al., 2005) and other modalities.

In the following, the nomenclature of Table 1 is explained:

- Time-res: Maximum time resolution in Hz. Given is the range for the sampling rate of the system. The lower value corresponds to the maximum sampling rate using the maximum number of sources and detectors. The higher value corresponds to the maximum sampling rate using a reduced set of channels. A slash (/) denotes two distinct sampling modes.
- #Emitter: Number of emitters. One emitter includes the whole set of wavelengths the device uses, which illuminate the same spot of the tissue. If a span is given, then the system uses a modular design and can be ordered in different configurations. If values are separated by a slash (/) then different types of NIRI sensors can be attached to the device.
- #Detector: Number of detectors. If a span is given, then the system uses a modular design and can be ordered in different configurations. If values are separated by a slash (/) then different types of NIRI sensors can be attached to the device.
- MUX: Multiplexing method to distinguish signals from different emitters and different wavelengths. (t)ime multiplexing (i.e. diodes are turned on during specific time-slots), (f)requency multiplexing (i.e. diodes are turned on permanently and different diodes are each modulated with a distinct frequency), (c)ode multiplexing (i.e. all diodes are turned on based on a different bit-sequence for each diode). A plus (+) indicates that two multiplexing techniques are used simultaneously.
- SDS: Source–detector-separation. Some devices use probes with predefined distances. If SDS can be adjusted freely by the user, then (a)djustable is written. Numbers represent fixed distances in mm. A plus (+) denotes that there are different distances present on a single NIRI sensor. If values are separated by a slash (/) then different types of NIRI sensors can be attached to the device. If a span is given, then the SDS of the NIRI sensor is adjustable in this range.
- E-tech: Emitter technology: Light emitting diode (LED) or (Laser) diode.
- Wavelengths: Default peak wavelengths used by the device. Parentheses "()" denote optional wavelengths and an asterisk (*) denotes that different wavelengths can be chosen.
- D-tech: Detector technology. PD: photodiode, APD: avalanche photodiode, PMT: photomultiplier tube.

- Data: Some devices provide raw light intensities (raw) or optical densities (OD), which can then be processed further with open source software like HomER2 (Huppert et al., 2009; PMILab, 2012) or user-implemented processing scripts. Other devices only deliver pre-computed [O_2Hb] and [HHb], which are much less suited for custom algorithms and open source tools.
- Wear: Wearable device. (y)es/(n)o: "y" means that the device is small enough to be carried by the subject him/herself and is battery operated to allow for studies including patient movement as in sports. "y*" denotes that data cannot be transmitted wirelessly from the wearable device to a host PC but is recorded in the device. Devices marked with "n" can be transported on a trolley.
- CE: Device is CE-marked. (y)es/(n)o: This is not mandatory when using the device for research purposes. But in general without CE mark, additional approvals by the authorities are required for experiments. A star (*) indicates that the device will be CE-marked in the near future.

Technological design aspects of fNIRI

From an engineer's point of view, CW fNIRI merely requires to switch on a NIR light source, couple the emitted light into the scalp, and measure the diffuse reflectance that re-emerges from the tissue a few centimeters distant from that source (Ferrari and Quaresima, 2012; Ferrari et al., 2004; Giacometti and Diamond, 2013; Hoshi, 2003; Strangman et al., 2002; Wolf et al., 2007). Hence, CW fNIRI instruments come in comparably simple setups, allowing specialization towards wearable, miniaturized and/or wireless applications, and can partially be built from off the shelf components at low cost (Flexman et al., 2012; Muehlemann et al., 2008; Q. Zhang et al., 2011; Vaithianathan et al., 2004). The technological aspects of the three major ingredients that are common to all CW fNIRI devices, i.e. NIR light (1) emitters, (2) detectors and (3) means to transport the light to/from the scalp, are discussed in the following.

Light sources for fNIRI instruments

Typically, two or a few more *discrete* wavelengths are used in NIRI, and the MBLL equations are evaluated at these selected wavelengths (Delpy et al., 1988; Kocsis et al., 2006). In broadband NIRI, however, light from a *continuous* portion of the spectrum is required in order to obtain the continuous absorption spectrum of the diffuse reflectance (Diop et al., 2009; Kashyap et al., 2007; Tisdall et al., 2007). To this end, broadband light sources are usually used, in combination with appropriate optical bandpass filters. For measuring only [O_2Hb] and [HHb] a higher SNR is achieved by using a few discrete, but well-chosen wavelengths (see Selection of optimum wavelengths section). Therefore this is the approach adopted by all commercial fNIRI instruments. For either approach, the emitted light needs to be from the NIR part of the spectrum in order to penetrate the tissue without being completely absorbed prior to detection (see discussion of the "optical window" in Selection of optimum wavelengths section).

In general, it is desirable to choose the radiated optical power as high as possible in order to maximize the amount of light at the detector, which leads to a higher SNR, and to be able to use longer source detector distance, which are more sensitive to deeper tissue. However, certain limitations apply. Tissue heating due to the irradiation and/or conductive heat transport from the source not only may distort the measurements, but may endanger or at least cause discomfort to the subject (Bozkurt and Onaral, 2004; Ito et al., 2000; Soraghan et al., 2008). More important, however, is proper safety for the eyes, for both, the experimenter and the subject. The power of the optical radiation reaching the brain tissue is low compared to natural exposure due to sunlight (Kiguchi et al., 2007) and poses no danger. Lasers are potentially more dangerous, because they can be pulsed and often emit a higher power than LEDs. The safety standards such as e.g. IEC 68025 or IEC 62471 and guidelines for lasers (International Commission on Non-Ionizing Radiation Protection, 2000) and LEDs (International Commission on Non-Ionizing Radiation Protection, 1997) pose limits on maximum output power (Sliney, 1997). Safety can be easily ensured by a proper design of the instrument. Commercial instruments generally implement these safety measures.

The light intensity emitted from a source usually fluctuates, and such fluctuations directly affect the noise at the detector (Zhang et al., 2001). For this reasons, light sources should radiate light as invariantly as possible. This applies to drift effects, i.e., changes in the emitted intensity of wavelength that vary slowly, e.g. due to temperature effects, as well as to pure emitter noise which may originate from a noisy power supply. A careful design of the power circuitry in order to reduce noise pickup as well as the stabilization of the power supply and even cooling of the light source help to reduce emitter noise.

For fNIRI measurements at several discrete wavelengths, it is desirable to choose light sources whose radiation spectra are as sharply peaked as possible; ideally being monochromatic light at one discrete wavelength. If the emission spectrum of the source is known, however, weighted averaging approaches exist to correct the extinction coefficients (and possibly also the differential path length factors) used for the MBLL (Muehlemann et al., 2008; Wahr et al., 1996; Zhang et al., 2001).

The wavelengths available for laser diodes (LDs) are limited, i.e. between 695 nm and 775 nm it is difficult to find laser diodes at a reasonable price and 760 nm is an absorption peak of HHb. Hence not all wavelengths are selectable. As shown later in this review, the selection of wavelengths can have substantial influence on the quality of measurement data (Selection of optimum wavelengths section). For miniaturized and/or wearable fNIRI instruments, the three factors size, weight and the power consumption play an important role in the selection of a particular light source. If fiber optic light guides are used to guide the light to or from the scalp, it is desirable to choose a source that allows for efficient coupling into the fibers.

Laser diodes (LDs) and light emitting diodes (LEDs) are the most widely used types of light sources that are employed in fNIRI instruments (see Table 1). In the remainder of this paragraph, they are compared against each other based on the aspects described above. Both, LDs and LEDs are based on semiconductor technology and exploit electroluminescence through radiative recombination of electron–hole pairs in the active region of forward-biased p–n-junctions (Liu, 2005). The emitted wavelength depends on the semiconductor material, as well as on its doping characteristics. While LEDs are based on spontaneous emission and thus emit incoherent light with a large bandwidth (typically 25–50 nm), LDs are based on stimulated emission, allowing for coherent light emission with a narrower bandwidth. LDs have a narrower operating range, while the intensity of LEDs is easy to adjust.

It becomes evident from Table 2 that LDs have the benefits of narrow spectral peaks with low divergence, which allows for easy coupling of the light into fibers. However, they often come in relatively large packaging, making miniaturization more challenging. Furthermore, the danger of laser radiation for the eyes must be addressed. LEDs are generally smaller than LDs, and are often considered a valid alternative to LDs. They come in a large variety of emitting wavelengths, hence allowing for more flexibility in the wavelength selection.

Table 2
Comparison of light emitting diodes (LEDs) and laser diodes (LDs). BW denotes spectral bandwidth and FWHM the full width at half maximum.

	BW (FWHM)	Size	Avail. colors	Divergence	Fiber coupling	Cost	Safety
LEDs	~35 nm	Small	Many	Broad	Possible	Low	Higher
LDs	<1 nm	Bulkier	Limited	Narrow	Easy	High	Lower

Selection of optimum wavelengths

To non-invasively determine [O_2Hb] and [HHb] with optimal SNR in tissue using fNIRI, the optical properties of both the tissue and of the O_2Hb and HHb have to be considered.

Regarding the medium, light in the near-infrared (NIR) spectral range (~650–950 nm, 'optical window') can propagate relatively deeply (a few centimeters) into biological tissue mainly, because NIR light is only weakly absorbed by water, hemoglobin, collagen and proteins (see Fig. 2). Light below 650 nm is too strongly absorbed by mainly hemoglobin and above 950 nm too strongly by water. In the spectral range of the 'optical window', O_2Hb and HHb have different minima and maxima in their absorption spectra, and an isosbestic point at ~800 nm (Zijlstra et al., 2000), where O_2Hb and HHb have the same absorption coefficient (Fig. 2). Although other substances have higher absorption coefficients in this range, they are only present at relatively low concentrations and consequently O_2Hb and HHb can be regarded as the main absorbers. Thus, the NIR spectral range is well suited to determine changes in [O_2Hb] and [HHb] non-invasively.

The selection of the specific wavelengths suited best to determine [O_2Hb] and [HHb] is a mathematical optimization problem which depends on a complex interplay between different variables, mainly (i) the number of wavelengths used, (ii) the number and type of chromophores considered, (iii) the model of the background medium (e.g. homogenous vs. non-homogenous, number of layers), and (iv) the mathematical approach to solve the optimization problem.

So far different methods have been developed for selecting the optimum wavelengths based on theoretical or experimental approaches. In the following, the different approaches and their results are briefly reviewed. An overview about the recommended wavelengths is given in Fig. 3.

Two wavelengths

Using an error propagation approach, Yamashita et al. (2001) showed that with the wavelength pair 664 nm and 830 nm [O_2Hb] or [HHb] can be determined twice or six times, respectively, more precisely compared to 780 nm and 830 nm (Yamashita et al., 2001) The latter pair is often used for NIRI. Yamashita et al. (2001) therefore recommend using 830 nm and a second wavelength in the range <780 nm, which is in agreement with other findings. Strangman et al. (2003) used a Monte Carlo simulation and considered three types of crosstalk (i.e. between [O_2Hb] and [HHb], from species-dependent pathlength factors, and between two different activation regions) in their optimization method. They showed that (i) 830 nm should be paired with 690 or 760, as well as that (ii) the wavelength range 770–800 nm provides only poor oxygenation information. Sato et al. (2004) tested empirically (on four subjects performing different cognitive and motor tasks) which of the four wavelengths 678, 692, 750 and 782 nm is the best combination with 830 nm to obtain an optimal SNR for both [O_2Hb] and [HHb]. 692 nm and 830 nm provided the highest SNR. Okui and Okada (2005) demonstrated in a Monte Carlo simulation by minimizing the crosstalk between [O_2Hb] and [HHb], that the optimal wavelength range for pairing with 830 nm for the dual-wavelength setup is between 690 nm and 750 nm. Funane et al. (2009) concluded from their theoretical analysis that the SNR is at its maximum when both ends of the range of 659–900 nm were used. In addition, they demonstrated that the SNR decreases when changes in the concentration of CtOx (i.e. [CtOx]) are included in the analysis. By using a Monte Carlo simulation, Kawaguchi et al. (2008) demonstrated the usefulness of the wavelength pair 690 nm and 830 nm in reducing the crosstalk between [O_2Hb] and [HHb].

Further investigations showed that the 830 nm wavelength may not be the optimal wavelength either. Uludağ et al. (2004b) concluded from their theoretical analysis of crosstalk between [O_2Hb] and [HHb] and separability (defined as a measure for the influence of physical noise on the [O_2Hb] and [HHb]) that for a dual-wavelength NIRI instrument, (i) not both wavelengths should be >780 nm, and (ii) the crosstalk is low and the separability high when one of the wavelengths is >730 nm and the other <720 nm. Correia et al. (2010) performed a detailed analysis of the two optimal wavelengths for NIRI by using a three layer model for the optical medium and three conditions for the optimization process: good separation between (i) absorption and scattering (i.e. maximum of the residual norm), (ii) [O_2Hb] and [HHb] (i.e. minimum of the condition number), and (iii) excellent overlap between the sensitivity profiles of the wavelength-dependent light paths in the medium (i.e. small sum of squared differences between the sensitivity profiles). The analysis revealed that the optimum wavelength pair is 704 ± 7 and 887 ± 12 nm.

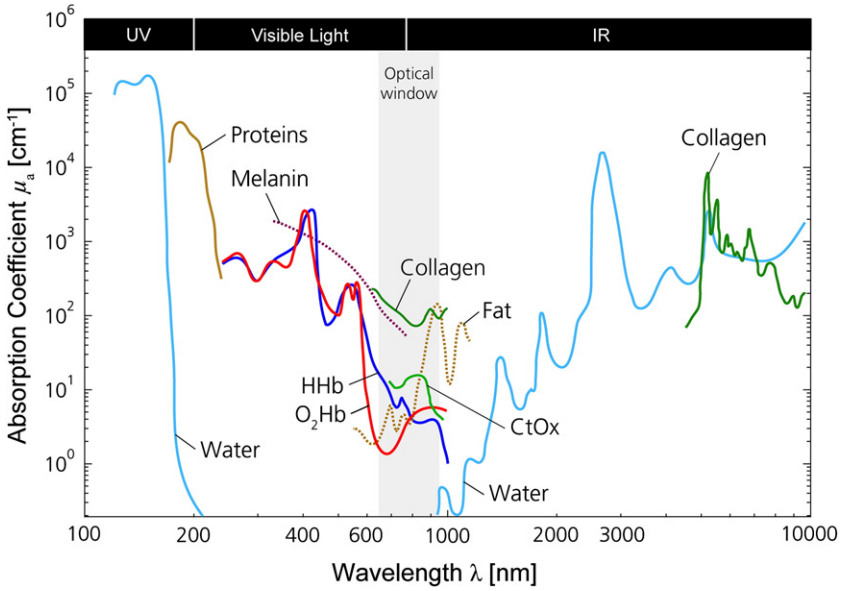

Fig. 2. Absorption spectra (natural logarithm base!) for different chromophores present in human tissue. Shown are the spectra for O_2Hb, HHb, proteins, water, collagen, fat and cytochrome oxidase (CtOx) in the region from 100 nm to 10,000 nm. The spectra are given with respect to the specific concentration in mM.
Data according to Obrig et al. (2000b), Taroni et al. (2007), Uludağ et al. (2004a), van Veen et al. (2004), Vogel and Venugopalan (2003) and Ward et al. (2006).

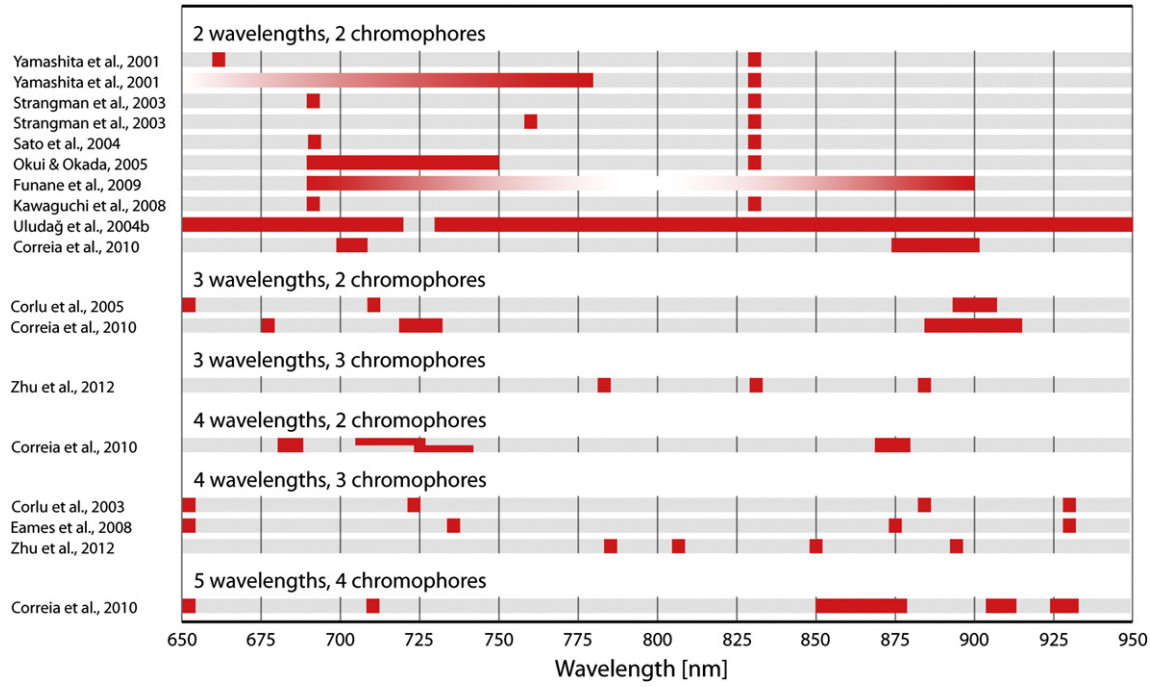

Fig. 3. Illustration of the recommended wavelength values in dependence of the number of wavelengths used and the number of chromospheres included in the analysis.

Three and more wavelengths

By simulating a medium with O_2Hb, HHb and H_2O as chromophores and by optimizing the residual norm and the condition number, Corlu et al. (2003) showed that when using *four* wavelengths, the optimum ones to separate between O_2Hb, HHb and H_2O are 650 ± 2, 722 ± 1, 884 ± 2 and 930 ± 2 nm. In a follow-up study, Corlu et al. (2005) added lipid as a fourth chromophore in the simulation and concluded that the optimum *five* wavelengths are 650 ± 3, 710 ± 1, 865 ± 15, 912 ± 4 and 928 ± 4 nm. In addition, they showed that when only assuming O_2Hb, HHb as chromophores in the medium and also allowing for scattering changes, the *three* optimal wavelengths are 650 ± 2, 716 ± 4 and 902 ± 16 nm. Using a similar simulation and analysis as Corlu et al. (2003), Eames et al. (2008) found 650, 736, 874 and 930 nm to be the optimum *four* wavelengths for determining O_2Hb, HHb and H_2O concentrations. Correia et al. (2010) improved the optimization approach used by Corlu et al. (2003, 2005) by incorporating a third condition in the optimization constraints (i.e. taking into account the interrogated volume of the light) and showed that for a simulated three layered medium with O_2Hb and HHb as chromophores the *three* wavelengths 680 ± 5, 725 ± 10 and 877 ± 12 nm or the *four* wavelengths 685 ± 7, 719 ± 9, 731 ± 8 and 873 ± 9 nm are optimal. Another approach for optimal wavelength selection was presented by Zhu et al. (2012). They measured cerebral changes in [O_2Hb], [HHb] and [CtOx] directly on piglets using a multi-spectral method and determined the optimal three or four wavelengths that minimize the normalized root mean square residual between the values determined by the multi-spectral method and by using only a finite number of wavelengths. They found that the *three* wavelengths 782, 832 and 884 nm, and the *four* wavelengths 786, 807, 850 and 889 nm are optimal.

In conclusion, the works mentioned in the previous sections show that (i) the optimum wavelength selection depends on the specific type of analysis performed and the assumptions made; (ii) for a two-wavelength fNIRI device the optimum wavelength in combination with 830 nm should be < 780; (iii) the optimum wavelength pair in general for a two-wavelength fNIRI device seems to be 704 ± 7 + 887 ± 12 nm (Correia et al., 2010), and (iv) different optimum wavelength combinations were proposed for more than two wavelengths, with the analysis performed by Correia et al. (2010) appearing to be the one based on the most realistic modeling approach so far, and the analysis of Zhu et al. (2012) seeming to be the most innovative one. Concerning the mathematical methods to determine the optimum wavelengths, it has to be stressed that unfortunately, to the best of our knowledge, none of them included superficial layers such as skin and scalp in their model. Since it was shown that the dark pigmentation of the hair and also the hair follicle strongly absorb light in the NIR wavelength range (McIntosh et al., 2010; Pringle et al., 1999), the optimum selection of wavelengths also has to take account of this issue in the future. Thus, the recommendations for optimum wavelength selection published so far should be regarded with reservation.

The discrepancy between the determined optimal values by Yamashita et al. (2001) and Correia et al. (2010) demonstrates that the type of optimization approach has a strong influence on the results.

One approach to circumvent the need for a selection process of optimum wavelengths could be to use the complete NIR spectrum rather than just a finite number of wavelengths to determine the concentration changes of chromophores. Devices and methods using this fNIRI multi-spectral (or broadband) approach are under development (e.g. Diop et al., 2009; Pucci et al., 2010; Srinivasan et al., 2007; Tachtsidis et al., 2008b, 2011, 2012; Xu et al., 2005). That the usage of the different spectral fitting methods has an effect on the measured concentration changes has been shown by Schelkanova and Toronov (2010). However, the multi-spectral approach is associated with two drawbacks, i.e. increased computational complexity and the need for reduced incident light power (compared to a normal fNIRI device) since light with a multi-spectrum has a higher total power than light with a restricted wavelength range. Theoretically, the highest SNR can be achieved by sampling at the two optimal wavelengths as often as possible.

Photodetectors for fNIRI instruments

Most photodetectors in photonic applications are based on the photoelectric effect (either internal or external), i.e. a photon generates free charge carriers, which in turn are detected as an electric signal (Liu, 2005).

The *external* photoelectric effect means that a photon frees an electron from the photocathode surface. In a photomultiplier tube

(PMT), this electron is accelerated by a strong electric field, such that its kinetic energy is high enough to knock out several secondary electrons from the surface of dynodes. This process is repeated in a cascade of dynodes, leading to a successive multiplication of the carriers, and hence results in high gains in the order of 10^6 to 10^7 (Liu, 2005).

The *internal* photoelectric effect means that the absorption of a photon by a semiconductor junction diode results in an electron–hole pair. These carriers are responsible for a photocurrent, which is again detectable as an electric signal. The photodiode (PD) is a prominent example of a photodetector that is based on the internal photoelectric effect. It has no internal signal amplification, and can be operated in either the photoconductive mode or the photovoltaic mode. In the photoconductive mode, a reverse voltage is applied across the junction and the resulting photocurrent is measured across a relatively small load resistance, resulting in an output voltage that is linear with the incident optical power. In the photovoltaic mode, no bias is applied and the load resistance is large, such that the photocurrent is negligibly small, resulting in a logarithmic response to the optical power (Liu, 2005). This can be of interest in fNIRI measurements, as the choice of different source detector separations can pose high demands on the dynamic range of the detector and the subsequent amplifier circuitry, which can be met by the logarithmic scale of the diode output. However, circuits operating in photovoltaic mode are much slower compared to photoconductive mode, because voltage changes are due to the tiny photocurrent generated by the photodiode divided by the input capacitance of the ensuing amplifier circuit.

Another example for a device that is based on the internal photoelectric effect is the avalanche photodiode (APD), which is, together with PDs, among the most widely used photodetectors in fNIRI instruments (see Table 1). By applying a large electric field across the APD junction, the charge carriers that are generated by photon absorption are accelerated and gain a kinetic energy high enough to generate more carriers through impact ionization, which in turn are accelerated and generate more carriers, etc. This leads to an avalanche type multiplication of carriers similar to a PMT which gives the APD its name and which results in an internal current amplification in the range of few hundred times (Liu, 2005).

Light sensors based on charge-coupled devices (CCD) are yet another group of photodetectors that make use of the internal photoelectric effect (Liu, 2005). CCDs are commonly used in broadband NIRI as part of the spectrometers needed to record the continuous absorption spectrum of the diffuse reflectance (Cope et al., 1989). Unlike single PDs or PMTs, the CCD sensor provides spatial information, i.e. it gives information about the distribution of the light intensity in an array of pixels (Janesick, 2001). In order to obtain a continuous spectrum, the incoming light is dispersed, normally by a diffraction grating. By measuring the intensity of the thereby spatially separated spectral components of the light on a CCD camera, the continuous spectrum of the diffuse reflectance is obtained (Cope et al., 1989).

In photodetector systems, there are mainly three different types of noise, i.e. *shot noise*, *dark current* and *thermal noise*. Shot noise is based on the quantum nature of the photons that enter the detector as well as the generated carriers, i.e. due to their stochastic non-uniform temporal distribution (Liu, 2005). Without internal amplification, the photonic shot noise power is proportional to the square root of the number of incident photons, as is the signal-to-shot-noise ratio. Thus, the more light enters the detector in a given time window, the more precise are the measurements. Shot noise is unavoidable; however, it can be minimized by carefully shielding the detector from background radiation (opaque cover and/or NIR bandpass filters). In devices with internal signal amplification, the *excess shot noise* describes the fluctuations that are due to the random multiplication effects inside the detector (Liu, 2005). The dark current is the current measured in dark conditions (no photons), e.g. due to thermal generation of electron–hole pairs in PDs. It can be reduced by cooling the device. Thermal noise is generally present in resistors internal and external to the detector and is due to Brownian motion of electrons. In detectors with internal gains, the photonic and dark current shot noise is amplified together with the signal; however, the thermal noise is typically small compared to the signal and becomes negligible.

The output signal of a detector is in general amplified and filtered prior to analog–digital conversion. In photodetectors without internal gain, the design and the component selection of the subsequent preamplifier circuitry must be carried out carefully in order to reduce noise pickup in circuit paths, wires, active components, etc. Detectors with internal gain reduce the requirements of the preamplifier components in terms of noise.

The three most important photodetectors used in fNIRI instruments—namely PD, APD and PMT—are compared in the following (Table 3).

Photodiodes have a high dynamic range in the range of 100 dB (Strangman et al., 2002), are easy to use since they usually do not need stabilized supply voltages or cooling, and come in small packages. Their speed is in the range of 100 MHz (Strangman et al., 2002), and they are not susceptible to magnetic fields, such as in fMRI scanners and robust to ambient light exposure. PDs, however, have no internal signal amplification; hence need low-noise preamplifiers that must be designed carefully. APDs have a moderate gains in the order of 100 (Liu, 2005), a dynamic range of 60 dB (Strangman et al., 2002) and come in small packages. They are robust to ambient light exposure and not sensitive to magnetic fields. Their operating voltage is in the order of tens to hundreds of volts. Due to the dependency of the internal gain on temperature and bias voltage, APDs require stabilized power supplies and are often cooled (Liu, 2005). APDs are faster than PDs and could be modulated with frequencies exceeding 100 MHz (Strangman et al., 2002). PMTs, while not very commonly used in fNIRI, represent the gold standard for photodetectors in terms of sensitivity, which allows for single photon counting. They exhibit large gains (up to 10^7) and high speeds similar to APDs (Strangman et al., 2002). The dynamic range of PMTs is in the range of 60 dB, comparable to APDs but lower than that of PDs (Strangman et al., 2002). Since the gain of PMTs is very sensitive to the (rather high) supply voltage, it must be stabilized (Liu, 2005). Furthermore, PMTs are large, and sensitive to magnetic fields, as well as highly vulnerable to exposure to ambient light. A possible alternative to PMTs was recently discovered in silicon photomultipliers (SiPMs), which essentially consist of APDs that operate in Geiger mode and hence exhibit photon counting capabilities (Renker, 2007). Being semiconductor-based devices, they come in small packages, require lower operating voltages and are not vulnerable to ambient light exposure or magnetic fields (Renker, 2007). Due to their practical advantages compared to PMTs, which we recently also started to discover with own experiments (Zimmermann et al., 2013a), we expect further developments employing SiPMs in the field of NIRI instrumentation.

Probe design

To transfer the light generated by the emitter to the scalp of the subject and the reflected light back to the detector, two options are available. The sources and detectors can be placed directly onto the

Table 3
Qualitative comparison of the most commonly used photodetectors, i.e. photodiodes (PD), avalanche photodiodes (APD) and photomultiplier tubes (PMT) in fNIRI devices. V_{op}: operating voltage (order of magnitude).

	Gain	Dyn. range	Size	V_{op}	Speed	Robustness	Susceptibility[a]
PD	None	High	Small	1 V	Medium	Good	No
APD	Moderate	Moderate	Small	100 V	Fast	Medium	No
PMT	Large	Moderate	Bulky	1 kV	Fast	Medium	Yes

[a] Susceptibility to ambient light exposure and/or magnetic fields.

skin (such as, e.g., in Bozkurt et al., 2005 or in Muehlemann et al., 2008), or the light can be guided by optical fibers to probes on the head (Fig. 4), where the fibers are fixed by appropriate fiber holders (Giacometti and Diamond, 2013). The means to guide light to the scalp (i.e. source fibers) is mostly composed of step-index multimode fibers with a core diameter in the range of 0.5 mm. Guiding the light from the scalp (i.e. to the detectors) usually involves fiber optic bundles with a larger diameter (e.g. 3 mm) and a high numeric aperture, in order to increase the amount of collected light. When sources and detectors are placed directly on the head, potential heating and electric hazards have to be prevented by the instrument, but the light coupling losses are minimal. When fiber optic light transmission is used, the added weight and inertia of optical fibers, losses due to fiber coupling and the reduced mobility of the subject are disadvantages (Ferrari and Quaresima, 2012; Wolf et al., 2007). However, fibers generally enable a more flexible geometrical design of a probe. It is important to ensure an optimal light coupling from the fibers to the scalp, both on the emitter and detector side. The more light is received, the higher is the SNR of the measurement. This light coupling depends to a large degree on hair color and density, and skin pigmentation (Strangman et al., 2002). Therefore it is important to carefully move hair away from detectors/emitters. Since the reflected light generally has a low intensity, detectors with larger active areas or fiber bundles are employed to increase the intensity of the collected light. However, the larger the detection area the more easily it can be obstructed by hair. Recently, the idea of using a fiber brush to overcome this drawback was proposed (Khan et al., 2012). In any case, care must be taken to prevent light from piping, i.e. the direct detection of light that never passed through tissue. Furthermore, changes in the contact pressure between optodes and the scalp lead to changes in light coupling and thus may introduce artifacts (Gibson et al., 2005; Wahr et al., 1996). This can be reduced by spring-loaded probes (Strangman et al., 2002).

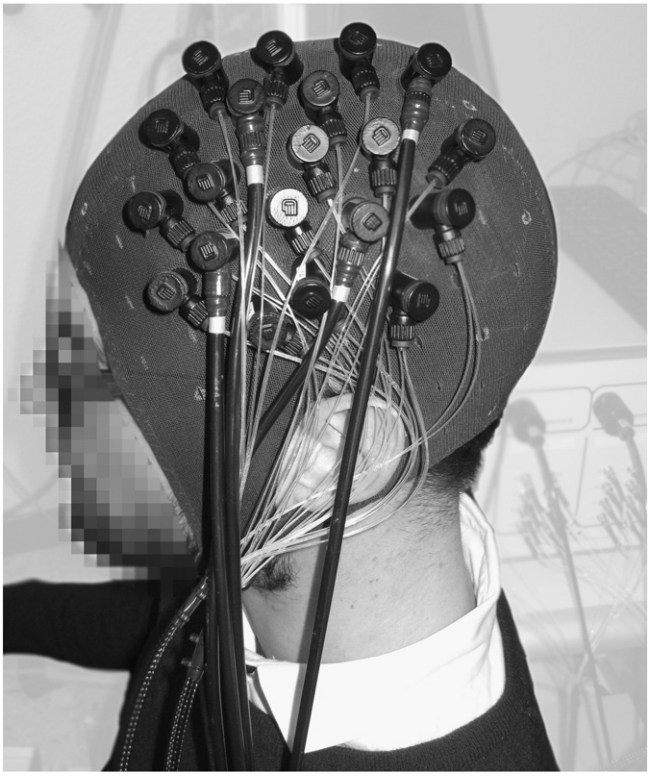

Fig. 4. Example of an experimental probe developed at the University Zurich and ETH Zurich. Spring-loaded fiber holders are fixed in an EEG cap. The thin source and thicker (black) detector fibers transmit the light from the instrument to the head and back. It is important that the probe is comfortable for the subject.

The question how to best arrange sources and detectors is not easy to answer. The aims of such an arrangement are to obtain a high image resolution, high sensitivity, accurate estimation of the chromophore concentrations, an effective elimination of the influence of superficial tissue layers and systemic physiological changes.

Early instruments were based on evenly spaced arrangements of sources and detectors with uniform source detector distance for all channels (e.g. Franceschini et al., 2003; Maki et al., 1995; Wolf et al., 2002). These approaches employed a simple backprojection algorithm, which offered a resolution in the order of the average distance between the midpoints of light bundles (Yamamoto et al., 2002). This approach yielded a map of cortical activity with a low quantitative accuracy and had the disadvantage of a high sensitivity to superficial layers of tissue (Boas et al., 2004). It is based on the assumption that changes only occur in the brain and not systemically.

An improvement to this approach was to include at least one short source detector distance in the order of 5 mm. Since the signals at short source detector distances are mostly affected by superficial tissue and hence by systemic physiological changes, this was an attempt to reduce the influence of these undesirable components (see Methods to separate different components in fNIRI signals section).

The next step was to move to tomographic approaches, i.e. an image reconstruction in three dimensions. This enables to remove the influence of superficial tissue, to obtain a higher sensitivity to deeper tissue and more accurate localization and quantification of the brain activity. It requires, however, that an instrument allows to measure at several different source detector distances with overlapping light paths and inherently means that the instrument needs a high dynamic range (Boas et al., 2004).

Culver et al. (2001) simulated the influence of the density of sources and detectors on the image resolution. They found that resolution depends on the SNR of the measurement, the depths of the object and density of sources and detectors. In particular, the higher the density of optodes, the higher is the resolution. This relationship is limited by the SNR of the instrument, i.e. a low SNR reduces the resolution due to noise. The deeper an object is, the lower is the achievable spatial resolution. They also tested a transmission geometry, which enabled higher resolution in deep tissues compared to a reflection geometry.

Since it is impossible to shine light through the whole adult human head, only sensors with reflection geometry are feasible for measuring brain activity. Boas et al. (2004) analyzed different reflection source/detector arrangements and found that including two distances and overlapping light paths increases the image resolution and localization accuracy. These simulations showed that a high dynamic range is required to implement this approach in an instrument. They favored the arrangement of sources/detectors in a hexagonal geometry, because it has lower requirements for the dynamic range compared to a rectangular geometry. Subsequently an instrument with the required specifications was built and the simulations were verified and indeed the tomographic approach led to a higher resolution and agreement with fMRI data compared to the backprojection approach (Joseph et al., 2006).

Tian et al. (2009) studied 6 different geometric arrangements of sources and detectors in a phantom experiment. They found that the most important factor affecting the resolution is the measurement density, i.e. the number of different light bundles interrogating a specific volume. The higher this measurement density is the higher is the image resolution that can be achieved. In addition, they showed that the image resolution and SNR have an asymptotic behavior with respect to the number of overlapping light paths, i.e. at a certain level the improvement becomes quite small which means there is an optimum density for the system complexity.

Dehghani et al. (2009b) simulated using NIRFAST high density arrays of NIRI. They found that an increase in the number of different source detector distances enables higher depth sensitivity, i.e. sensitivity to brain tissue at greater depths than 20 mm. This would enable

the detection of activation even in sulcal folds. From the instrumentation point of view this means that an extremely high dynamic range is required to implement these simulation results in a real system.

Analysis of fNIRI signals

Approaches to determine the [O_2Hb] and [HHb]

There are different algorithms to convert raw light intensity data into [O_2Hb], [HHb] and the total hemoglobin concentration ([tHb], i.e. the sum of [O_2Hb] and [HHb]) or tissue oxygen saturation (StO_2). The most common ones in fNIRI are the MBLL (Delpy et al., 1988) and multi-distance (MD) approaches, making use of several source–detector distances.

In the following we will discuss properties and assumptions of the different approaches. Independent of the approach when using CW devices it is not possible to determine absolute concentrations for O_2Hb and HHb, and thus tHb, because μ_s' cannot be measured directly. All approaches are assuming a homogenous tissue for the investigated area, which is not true for investigations of functional brain activity and this leads to errors in quantification, but the qualitative trend of the concentration change normally is still correct and therefore this approach is used in fNIRI (see further discussion below in Modified Beer–Lambert Law (MBLL) and Methods to separate different components in fNIRI signals sections). These approaches also require that μ_s' is much larger than μ_a which generally holds true for tissue.

The MBLL furthermore assumes that μ_s' does not vary with time and that changes in detected light intensity can be mainly attributed to changes in [O_2Hb] and [HHb]. These assumptions are similarly true for MD approaches, which are explained below. MD algorithms can give a reliable and stable measurement for the StO_2, which was clinically applied e.g. for monitoring premature neonates, as their brain is very sensitive to both too high and too low oxygen levels in the brain (Wolf et al., 2012). The MBLL and a short notice on its extensions using multi-spectral measurements will be discussed first (Modified Beer–Lambert Law (MBLL) section), while MD based approaches enable a depth resolution and are therefore discussed in Multivariate methods of type 1 section.

Modified Beer–Lambert Law (MBLL)

The MBLL (Delpy et al., 1988) extends the Beer–Lambert law by introducing a scattering dependent light intensity loss parameter, here denoted by G. The law describes the loss of light intensity (I) in tissue (optical density OD, also sometimes attenuation A, unitless) as a function of the chromophore concentrations (c, units [M]), molar extinction coefficients (ε, [M^{-1} cm^{-1}], not to be mistaken with the molar absorption coefficient $\alpha = \ln(10)\varepsilon$ or the absorption coefficient $\mu_a = \alpha c$), differential path length factor (DPF, unitless; accounts for the increased distance the light travels due to μ_s'), source–detector separation (d, [cm]) and G (unitless):

$$OD(t,\lambda) = -\log_{10}\left(\frac{I(t,\lambda)}{I_0(t,\lambda)}\right) = \sum_i \varepsilon_i(\lambda) c_i(t) DPF(\lambda) d + G(\lambda). \quad (1)$$

The index i denotes all investigated chromophores, commonly [O_2Hb] and [HHb] and I_0 denotes the intensity of the emitted light. Also note that in Eq. (1) we use the base 10 logarithm (i.e. $I = I_0 10^{-\varepsilon c d}$) and therefore use molar extinction coefficients, rather than the absorption coefficients which are associated with the natural logarithm. Both represent the level of absorption per concentration (μM/mM) and per length (cm) but differ by a scaling factor of ln(10) (Matcher et al., 1995a; UCL, 2005). Assuming that the change in scattering is small compared to the change in absorption, G can be assumed to be time-invariant. Hence it can be neglected when determining the change in optical density ($\Delta OD(\Delta t,\lambda) = OD(t_1,\lambda) - OD(t_0,\lambda)$) for a time point t_1 against an initial time point t_0. In addition, we assume that the emitted intensity I_0 is constant and therefore this term cancels out.

$$\Delta OD(\Delta t,\lambda) = -\log_{10}\left(\frac{I(t_1,\lambda)}{I(t_0,\lambda)}\right) = \sum_i \varepsilon_i(\lambda)\Delta c_i DPF(\lambda) d, \quad (2)$$

where $\Delta c_i = c_i(t_1) - c_i(t_0)$ is the temporal change in chromophore concentration. The MBLL is valid for a homogenous change in [O_2Hb] and [HHb] in homogenous tissue. As mentioned above, this approximation does not hold true for measurements of the head, as discussed by e.g. (Boas et al., 2001; Obrig and Villringer, 2003). The fact that the head is inhomogeneous is not a problem, because the inhomogeneity remains constant and is mostly covered by the constant G, which cancels out for measuring concentration changes. The fact that the concentration change in O_2Hb and HHb is not homogenous, i.e. it occurs only in the brain and not in other tissues such as skin and skull, leads to an error in quantification, i.e. the MBLL strongly underestimates the size of the changes in [O_2Hb] and [HHb]. In principle this error can be corrected, by taking partial differential pathlengths into account (Hiraoka et al., 1993), but usually this correction is not performed, because the trend of the signals is correct and quantification is not important in brain research, i.e. it is sufficient to detect, whether an activation is present or not, where the activation is occurring and signals can certainly be compared between different locations or different stimulations paradigms.

The values for ε and DPF can be found in the literature (e.g. Duncan et al., 1995; Matcher et al., 1995a). The DPF was found to be age, gender and wavelength dependent and varies between subjects (Duncan et al., 1996; Essenpreis et al., 1993) and different tissues (Duncan et al., 1995). For example the average DPF for the adult head for 100 subjects given by Duncan et al. is 6.53 ± 0.99, i.e. 15% variability between subjects. Since it is inversely proportional to the concentration change this will lead to an error of 15% in the estimation of the concentration change for an individual subject. This error could be corrected by applying time resolved instrumentation that is able to measure the DPF or by broadband spectroscopy, which is able to estimate the optical pathlength (Matcher et al., 1994). But the use of time resolved instrumentation is more expensive and complicated and quantification is not so important. In addition, the large majority of research is performed in groups of subjects/patients and results are presented in terms of group averages. In this case this error is averaged out and no longer relevant. Since there are different values for the DPF in the literature, it is necessary to state in each publication, which DPF values were applied. This also enables comparability between publications.

To finally obtain the hemoglobin concentration changes, Eq. (2) is evaluated at 2 wavelengths and the resulting system of equations solved for Δc, i.e. Δ[O_2Hb] and Δ[HHb]:

$$\begin{bmatrix}\Delta[\mathrm{HHb}]\\ \Delta[\mathrm{O_2Hb}]\end{bmatrix} = (d)^{-1}\begin{bmatrix}\varepsilon_{\mathrm{HHb},\lambda_1} & \varepsilon_{\mathrm{O_2Hb},\lambda_1}\\ \varepsilon_{\mathrm{HHb},\lambda_2} & \varepsilon_{\mathrm{O_2Hb},\lambda_2}\end{bmatrix}^{-1}\begin{bmatrix}\Delta OD(\Delta t,\lambda_1)/DPF(\lambda_1)\\ \Delta OD(\Delta t,\lambda_2)/DPF(\lambda_2)\end{bmatrix} \quad (3)$$

Instead of integrating the wavelength dependent DPF and the distance into OD matrix, it is also common to include these parameters in the extinction coefficient matrix and to state the resulting numbers, e.g. Matcher et al. (1995a). These numbers are only true for a specific instrument with specific wavelengths. In fact, even though a lot of instruments use the MBLL, the implementation differs from instrument to instrument. The MBLL can also be derived in a slightly different form from the diffusion approximation (Sassaroli and Fantini, 2004).

The time-differential MBLL approach can be extended using a multi-spectral approach. In this approach the OD difference is calculated between two wavelengths (measurement wavelength − reference wavelength). This was used e.g. to measure changes in cytochrome oxidase redox state in a rat brains without knowledge of its absorption spectrum (Hoshi et al., 1997). This approach is also known as SAPPORO

algorithm (Hazeki and Tamura, 1989). A similar approach is also able to determine absolute values for StO_2, [O_2Hb] and [HHb] (Benni et al., 2005), but requires a one-time calibration against blood samples.

Methods to separate different components in fNIRI signals

The signals measured by fNIRI and other modalities (e.g. fMRI) are contaminated with signal components that are not associated with functional brain activity, which may mask the brain activity. For this reason, fNIRI (like fMRI) studies usually include repetitions of stimulations. To improve the SNR it would be desirable to remove signal components that are not associated with brain activity. An effective removal increases the SNR, and enables to reduce the number of subjects and repetitions and the measurement time, possibly to a single trial. In the following we will discuss methods to remove undesired signal components.

Classification of signal components

The non-stationary fNIRI signals, i.e. [O_2Hb], [HHb], [tHb] and StO_2, are a combination of (i) evoked neurovascular coupling by a stimulus/task, (ii) non-evoked (i.e. spontaneous) neurovascular coupling, and (iii) processes that are not induced by neurovascular coupling, i.e. evoked and non-evoked systemic physiological processes ('physiological interference' or 'systemic interference'). In general, the changes present in fNIRI signals recorded on a human head are composed of different components that can be classified according to three aspects: (i) *source* (intracerebral vs. extracerebral), (ii) *stimulus/task relation* (evoked vs. non-evoked), and (iii) *cause* (neuronal vs. systemic).

According to the anatomical and physiological constraints, this classification leads to six signal components (SC1–SC6) that are, in principle, present in every recorded fNIRI signal (see Table 4).

Components caused by cerebral neuronal activity (SC1, SC4). Functional brain activity (SC1) in fNIRI signals originates from evoked *local neurovascular coupling* (Buxton, 2012; Devor et al., 2012) and is directly related to functional brain activity (see Table 4). The signal changes associated with this component are small (i.e. ~0.5 μM for [O_2Hb], ~−0.2 μM for [HHb] (Wolf et al., 2002)) in relation to the overall variability of the fNIRI signals (in general ~1 μM for [O_2Hb] as well as [HHb]). The component is generally termed "stimulus/(or task)-evoked hemodynamic response" and its extraction from the fNIRI signals is of primary interest in most fNIRI studies. In order to designate this component more precisely we suggest using the term "neuronal hemodynamic response" (associated with SC1) in contrast to "systemic hemodynamic response" (SC2–3). A typical neuronal hemodynamic response is shown in Fig. 5a. Fig. 5b visualizes the physiological processes involved, according to (Buxton, 2012; Devor et al., 2012).

As a second component (SC4), spontaneous brain activity (i.e. non-evoked) is also associated with neurovascular coupling and contributes to the variability of fNIRI signals. This component can be used to assess the so called "resting-state functional connectivity" of the brain (Greicius et al., 2009; Raichle, 2009; Sasai et al., 2012; White et al., 2009), which can be directly measured using electroencephalography (EEG) or magnetoencephalography (MEG), and indirectly using fNIRI, magnetic resonance imaging (fMRI) or positron emission tomography (PET). The type of functional connectivity measured using EEG or MEG (i.e. the '*neuronal* functional connectivity') should not be confused with this connectivity-type measured using fNIRI, MRI or PET (i.e. the '*vascular* functional connectivity'), as highlighted by Wolf et al. (2011).

Components caused by cerebral and extracerebral systemic activity (SC2–3, SC5–6). The reflection geometry commonly used in fNIRI is very sensitive to the extracerebral compartment of the head (i.e. scalp skin, subcutaneous tissue, aponeurosis, connective tissue, periosteum, cranium, meninges (dura mater, arachnoid mater, pia mater), cerebrospinal fluid (CSF) (Ellis, 2012)) since the light is both introduced and collected at the surface of the scalp. For a single source–detector arrangement, it was shown the light intensity is ~10–20 times (depending on the model for estimating the hemodynamic signals and the SDS) more sensitive to the extracerebral compartment compared to the cerebral compartment (Al-Rawi et al., 2001; Liebert et al., 2004). The tissue-specific energy of light absorbed in the head by using a 3 cm SDS was investigated by Haeussinger et al. (2011) by a Monte Carlo simulation based on three-dimensional segmented structural MRI data. They showed that the main part of the energy is absorbed by the extracerebral compartment (scalp: ~76%), skull: ~20%, CSF: ~0.4%) compared to the cerebral one (gray matter: ~3%, white matter: ~0.0005%). Please note that all these considerations are only true for single source detector separations and that an MD, imaging or tomography approach substantially reduces the influence of superficial tissue (Multivariate methods of type 1 section).

Depending on the stimulus/task relation and the type of compartment, the following systemic components present in fNIRI signals have to be distinguished:

(i) Evoked systemic cerebral (SC2) and extracerebral (SC3) activity: From physiology, it is known that one of the strongest parameters affecting in cerebral blood flow (CBF) and volume (CBV) is the partial pressure of carbon dioxide in the arterial blood ($PaCO_2$), commonly determined by measuring the end-tidal carbon dioxide ($P_{ET}CO_2$). $PaCO_2$ strongly affects the blood vessel diameter, especially of large arteries and small arterioles. E.g. a decrease in $PaCO_2$ (hypocapnia) leads to a reduction in CBF and CBV by vasoconstriction (Poeppel et al., 2007; Szabo et al., 2011). How $PaCO_2$ affects fNIRI signals was reviewed by Scholkmann et al. (2013) and how to model the coupling between $PaCO_2$, blood pressure (BP) and cerebral hemodynamics/oxygenation can be found in (Payne et al., 2011). Durduran et al. (2010) demonstrated that $PaCO_2$ changes affect the cerebral and extracerebral compartment differently, i.e. an increase in $PaCO_2$ (hypercapnia) led to a significant increase in CBF, but only to a negligible increase in scalp blood flow (SBF). Scholkmann et al. (2013) showed that $PaCO_2$ changes were evoked by speech and mathematical tasks, and strongly affected the fNIRI signals.
Task execution may also lead to significant changes in BP during certain experimental tasks such as arm-rising (Minati et al., 2011), anagram task (Tachtsidis et al., 2008a,c, 2009), word generation and constructional puzzle task (Moody et al., 2005),

Table 4
Classification of main components present in fNIRI signals. SC#: signal component #.

	Evoked		Non-evoked	
	Neuronal	Systemic	Neuronal	Systemic
Cerebral	SC1 Functional brain activity (neurovascular coupling)	SC2 Systemic activity type 1 (e.g. changes in blood pressure, $PaCO_2$, cerebral blood flow/volume)	SC4 Spontaneous brain activity (neurovascular coupling)	SC5 Systemic activity type 3 (e.g. heart rate, respiration, Mayer waves, very low frequency oscillations)
Extracerebral	–	SC3 Systemic activity type 2 (e.g. changes in blood pressure, skin blood flow/volume)	–	SC6 Systemic activity type 4 (e.g. heart rate, respiration, Mayer waves, very low frequency oscillations)

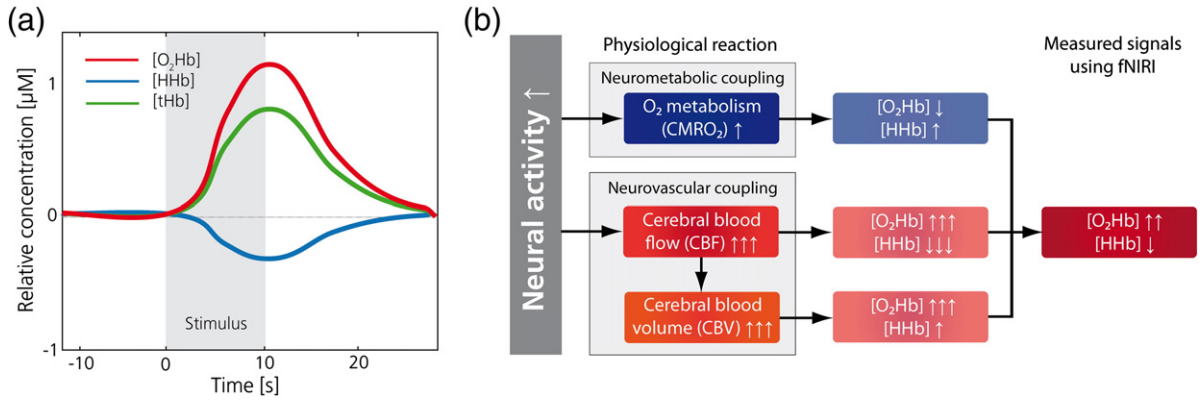

Fig. 5. (a) Typical evoked changes in cerebral oxygenation and hemodynamics due to an increase in brain activity. (b) Overview of the cerebral hemodynamic and oxygenation changes and their effect on the NIRI-derived signals in case of an increased neural (brain) activity. [O_2Hb] : oxyhemoglobin concentration, [HHb] : deoxyhemoglobin concentration and [tHb] : total hemoglobin concentration.

semantic continuous performance task (Jelzow et al., 2011), or emotional picture presentation (Minati et al., 2009). These BP changes affect hemodynamics in the extracerebral compartment, measured as stimulus/task-related changes in SBF and/or volume (SBV) (Kirilina et al., 2012; Takahashi et al., 2011), or even in the cerebral compartment itself (Minati et al., 2011). Takahashi et al. (2011) emphasized that a major part of the evoked changes in [O_2Hb], measured in the forehead during a cognitive task, is due to evoked changes in the SBF. This underlines that it is recommendable to either apply methods to reduce the influence of superficial tissue (Multivariate methods of type 1 section) or employ stimulations that do not change the BP. Another source of systemic component is the influence of the autonomic nervous system (ANS) on the cerebral vasculature (Hamel, 2006; Wahl and Schilling, 1993). For example, Giller et al. (2000) showed that a rhythmic handgrip exercise causes a sympathetic-mediated modulation of the hemodynamics in the middle cerebral artery. Cerebral hemodynamics is also affected by parasympathetic and trigemino-vascular activity (Goadsby et al., 1997; Wahl and Schilling, 1993). The superficial layer of the extracerebral compartment, i.e. the skin, is also under the influence of the ANS; a good example for this is facial flushing (Drummond, 1999; Drummond and Lance, 1987), which takes place even during a simple static handgrip task (Giller et al., 2000), for example. Kirilina et al. (2012) suggest that stimulus/task-evoked sympathetic arterial vasoconstriction may influence fNIRI signals. The concrete meaning of ANS related changes for fNIRS studies is an important topic for future investigations.

Another study showed that also the hemoglobin concentration and the hematocrit (i.e. the volume percentage of red blood cells in blood) can change during a challenging task (e.g. acute mental stress) (Muldoon et al., 1992). However, it should be noted that the duration of the task was 20 min indicating that this kind of physiological effect is relevant only for long tasks. Furthermore, unintentionally performed stimulus/task-evoked movements of the head may lead to movement artifacts. These are mostly due to changes in light coupling to the tissue, but part could also be due to genuine changes in CBF/CBV, in the fNIRI signal (Izzetoglu et al., 2005; Kurihara et al., 2003; Özgören et al., 2012; Scholkmann et al., 2010; Takahashi et al., 2012; Tax et al., 2011). That also the saliva secretion rate is accompanied with changes in extracerebral hemodynamics was initially shown by Sato et al. (2011) and recently confirmed by Matsumoto et al. (2012).

(ii) Non-evoked systemic cerebral (SC5) and extracerebral (SC6) activity:

A relatively large amount of the variability in fNIRI signals is not primarily stimulus/task-related but originates from changes in hemodynamics or vasomotion (i.e. variations in the blood vessels diameter) associated with *spontaneous hemodynamic oscillations* in different frequency bands as such as the cardiac signal (i.e. heartbeat, ~1 Hz), respiration (~0.3 Hz), low frequency (LF) (Mayer wave) (~0.1 Hz) and very low frequency (VLF) oscillations (<0.1 Hz) of different physiological origin (Cheng et al., 2012; Julien, 2006; Obrig et al., 2000a; Phillip et al., 2012; Reinhard et al., 2006; Tong et al., 2011; Toronov et al., 2000; Trajkovic et al., 2011). Also oscillations in the CSF (Droste and Krauss, 1997; Feinberg and Mark, 1987; Friese et al., 2004; Gupta et al., 2010; Kao et al., 2008; Strik et al., 2002) and even periodic displacements of the brain itself (Enzmann and Pelc, 1992; Feinberg and Mark, 1987; Poncelet et al., 1992; Soellinger et al., 2007, 2009) may contribute to the non-evoked signals. Spontaneous hemodynamic oscillations are present in the cerebral and extracerebral compartment (Habermehl et al., 2012b). Although there are many studies demonstrating the systemic origin of the spontaneous hemodynamic oscillations, Hoshi et al. (1998) found that these oscillation are also related to neuronal brain activity.

Despite the fact that the spontaneous hemodynamic oscillations (i.e. heartbeat, respiration, LF, and VLF) are not stimulus/task-evoked themselves, their characteristics (i.e. amplitude, frequency, phase) can be modulated by the stimulus/task to some degree. For example, it was shown that the amplitude of LF and VLF oscillations depend on the activity state (rest vs. task) (Obrig et al., 2000a), sleep stage (Näsi et al., 2011), body posture (Tachtsidis et al., 2003, 2004), or age of the subject (Peng et al., 2008; Safonova et al., 2004). Thus, although these oscillations arise spontaneously, their stimulus/task-evoked modulation capability leads to the conclusion that they may also be part of the systemic activity type 1 and type 2 (SC2–3). Toronov et al. (2000) even concluded that the activation signals detected by fNIRI and fMRI are mainly due to a synchronization of spontaneous oscillations with the stimulation rhythm.

Challenges for classification and separation of the signal components

The major challenge in separating the different signal components in fNIRI signals is the fact that all the evoked and non-evoked, neuronal and systemic hemodynamic changes do not take place as separate and non-influenced processes but form an interactive network of interlinked processes. E.g. this is demonstrated by the findings that the *amplitude* variations of the spontaneous LF oscillation can be caused by *frequency* variations of respiration. Respiration with the

same frequency as the LF oscillation (0.1 Hz) leads to a resonance amplification (Cheng et al., 2012; Diehl et al., 1995; Obrig et al., 2000a; Reinhard et al., 2006) and the choice of the length of the stimulation period influences the amplitude substantially (Toronov et al., 2000). Furthermore the LF oscillation seems to be interconnected with stimulus/task-evoked functional brain activity (i.e. hemodynamic responses) (Wolf et al., 2011), which led the authors to the conclusion that "functional cerebral hemodynamics can also be considered as a nonlinear synchronization phenomenon"—a conclusion that questions that the measured hemodynamic changes are caused by functional brain activity and proposes that they are caused by stimulus/task-related modulation of spontaneous hemodynamic oscillations.

Based on these findings, the classification and separation of fNIRI signals is a challenging task. The presented classification scheme (Table 4) should be regarded as generalized guidance in order to classify and assess the different fNIRI signal processing methods developed so far.

Mathematical and technical methods to separate the signal components

Methods developed to date to separate the different components in fNIRI signals can be classified into three categories: (i) *univariate methods*, (ii) *multivariate methods of type 1*, and (iii) *multivariate methods of type 2*. Whereas the univariate methods use only one single signal, the multivariate ones use more than one to perform the signal separation. The multivariate methods can be distinguished into two subtypes according to their usage of fNIRI signals alone (type 1) or also of additional non-fNIRI signals (type 2).

Univariate methods

A common practice in fNIRI signal processing is to band-pass or low-pass filter the signals in order to remove non-evoked (i.e. SC4–6) components (e.g. Franceschini et al., 2003; Spichtig et al., 2012). For example, a cutoff frequency of 0.2 Hz is commonly used.

To adaptively remove the heartbeat from the fNIRI signals, Gratton and Corballis (1995) developed an adaptive average waveform subtraction algorithm, and Biallas et al. (2012) and Trajkovic et al. (2009, 2011, 2012) presented an approach based on factor graphs. Further methods based on wavelet filtering (Jang et al., 2009; Lina et al., 2008, 2010; Matteau-Pelletier et al., 2009) were proposed. Y. Zhang et al. (2010) developed a method using empirical mode decomposition (EMD) and Hilbert spectral analysis to adaptively filter fNIRI signals. X. Zhang et al. (2012) used wavelet coherence analysis to identify evoked changes in fNIRI signals. Besides these filtering approaches, probably still the most widely used method to remove the components SC4–6, is 'conventional averaging' (CA), an average of segments of the fNIRI signal that are time-locked to the presented stimuli. This is also called block averaging or time triggered averaging. An improved version based on Bayesian filtering, outperforming the CA, was presented recently by Gagnon et al. (2014) and Scarpa et al. (2010). All these methods have the disadvantage that they do not enable to separate the components SC1–3 from each other, primarily because the frequency bands of the components SC1–3 overlap with those of SC4–6.

Multivariate methods of type 1

To overcome the limitations of the univariate methods, a great variety of different multivariate methods have been developed over the last decades. It was recognized quite early in the fNIRI research that using the information of fNIRI signals originating from different SDS (multi-distance; MD NIRI) helps to substantially reduce effects from superficial absorption changes (SC3 and SC6). There is a variety of such MD methods, which is discussed in Spatially resolved and self-calibrating probe multi-distance approaches section. Later tomographic imaging approaches, which are also based on measurements at different distances, enabled an image resolution also in depths of the tissue and thus further enhance the possibility to remove effects of extracerebral tissue (SC3 and SC6) and are discussed in Probe design and Depth resolution by imaging approaches sections. There are also several signal processing frameworks, which among other features take into account the information of MD fNIRI to extract functional brain activity (SC1). These approaches are based on biomedical signal analysis and are discussed in Signal analysis methods to extract the functional brain activity section.

Spatially resolved and self-calibrating probe multi-distance approaches. MD NIRI is based on a mathematical framework that relies on the theory of light propagation in a semi-infinite medium and analyzes the slopes of the decrease in light intensity as a function of SDS (Fantini et al., 1994; Matcher et al., 1995b; Suzuki et al., 1999). MD NIRI approaches were developed for CW as well as frequency-domain (FD) NIRI. In the following we will discuss MD fNIRI methods developed.

The MD approach generally implies that the tissue is measured at several distances at the same time. Several such approaches have been developed to calculate StO_2, an absolute value. The two main types of developed MD methods are *spatially resolved spectroscopy* (SRS) and the *self-calibrating* (SC) *method*.

While oxymetry systems from Hamamatsu Photonics (Hamamatsu, Japan) implement SRS (Matcher et al., 1995b; Suzuki et al., 1999), ISS Inc. uses the SC method (Hueber et al., 1999). Both approaches determine absolute values of StO_2, but while the ISS system based on FD technology measures the μ_s' and thus provides absolute values of [O_2Hb], [HHb], [tHb] too, the SRS system has to assume a reasonable value for μ_s'. StO_2 is also called "tissue oxygenation index" or "regional oxygen saturation index" in the literature. It is usually used as oximetry for monitoring and not for fNIRI. But compared to the MBLL approach, MD NIRI methods have several advantages: (i) They provide absolute values, which are more robust against movement artifacts compared to the time differential MBLL measurements. In the MBLL approach, a change in light coupling is misinterpreted as a change in [O_2Hb] and [HHb], while for the MD approach a change in coupling usually affects all distances similarly and therefore cancels. (ii) Calculating the change in light intensity over distance removes the influence of superficial tissue automatically (Franceschini et al., 1998) and consequently is more sensitive to the brain.

CW technology cannot measure μ_s', but if a reasonable assumption is made for μ_s', absolute concentrations of [O_2Hb], [HHb], [tHb] and StO_2 are obtained. Although this approach still requires assuming that the tissue and change in [O_2Hb] and [HHb] are homogenous, which is still not completely fulfilled, this assumption is more valid compared to the single source detector distance approach, because the superficial tissue layers are removed by the MD approach.

The SRS method measures at least at two SDS, i.e. one source in combination with at least two detectors (or vice versa), which are close together (see Fig. 6b). From the intensity I values measured at the different detectors an attenuation slope $\partial A/\partial d$, where $A = -\log_{10}(I/I_0)$, is calculated and inserted in the following equation to calculate the μ_a of the tissue (Suzuki et al., 1999):

$$k\mu_a(\lambda) = \frac{1}{3(1-h\lambda)}\left(\ln(10)\frac{\partial A(\lambda)}{\partial d} - \frac{2}{d}\right)^2. \quad (4)$$

This equation is based on a solution of the diffusion approximation for a semi-infinite homogenous medium and a short pulse from a point source (Patterson et al., 1989). [O_2Hb] and [HHb] are calculated as in Eq. (3). The μ_s' is modeled to decrease linearly over the wavelength range $\mu_s' = k(1-h\lambda)$. Since the parameter k will cancel out when calculating $StO_2 = k[O_2Hb] / (k[O_2Hb] + k[HHb])$ and the parameter h is similar for different kinds of tissue and different subjects and given in (Suzuki et al., 1999). With a reasonable assumption for μ_s' absolute [O_2Hb] and [HHb] can be calculated. Note that $\partial A/\partial d$ only becomes approximately linear for longer distances. In addition, the detectors need

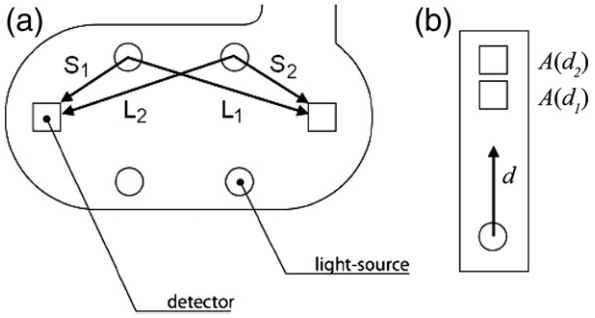

Fig. 6. a) Example of a source–detector arrangement for the self-calibrating approach. Arrows indicate the paths used to calculate the [O_2Hb], [HHb], [tHb] and StO_2 and point from source to the detector. b) Example arrangement for the spatially resolved spectroscopy approach.

to be placed close together, so that the different light paths probe the most similar volume.

The SC approach (Hueber et al., 1999) enables to compensate for time varying differences in light coupling by employing at least two sources and two detectors, which are arranged symmetrically. Each source has a separation d_L to one detector and d_S to the other detector, with $d_L > d_S$. The slope *Sl* of the decrease in light intensity *I* with the increasing distance is calculated using following equation (Hueber et al., 1999):

$$Sl = \frac{\frac{1}{2}\ln\left(\frac{I_{L1}I_{L2}}{I_{S1}I_{S2}}\right) + 2\ln\left(\frac{d_L}{d_S}\right)}{(d_L - d_S)}. \quad (5)$$

The indices L_1, L_2, S_1 and S_2 denote the different source–detector paths (Fig. 6a) and I_{L1}, etc. being the measured intensity from this source detector pair.

Due to the symmetry, the coupling factors of each source and detector appear both in the denominator and numerator and thus conveniently cancel out. Note that the slope is linear also for shorter distances and is wavelength dependent. The slope is related to μ_a as follows:

$$Sl_{dc} = -\sqrt{\frac{\mu_a}{D}}. \quad (6)$$

D is the diffusion coefficient $D = 1 / (\mu_a + \mu_s') \approx 1 / \mu_s'$. [$O_2$Hb] and [HHb] are calculated as in Eq. (3) by assuming a value for μ_s', which can be found in e.g. (Matcher et al., 1997). This approach is also based on a solution of the diffusion approximation for a semi-infinite homogenous medium for a point source (Fantini et al., 1994).

Since changes in light coupling often occur during movements, the advantage of this approach compared to MBLL and SRS is that the coupling factors cancel out and thus the influence of movement artifacts is much reduced. Also a potential drift of the light sources and detector sensitivity cancel out.

It was shown that MD fNIRI based changes in [O_2Hb], [HHb], [tHb] and StO_2 are only slightly influenced by changes in SBF/SBV induced by an extracarotid artery clamp (Al-Rawi et al., 2001), and the MD fNIRI methodology is superior to the traditional MBLL approach in excluding extracranial hemodynamic changes (Canova et al., 2011); but MD fNIRI does not completely remove changes in the extracerebral compartment (Davie and Grocott, 2012). The original MD NIRI approach was extended to two-layer models (Choi et al., 2004; Fabbri et al., 2004) and ultimately to five-layer models (Yamada et al., 2009, 2010), the last one including also μ_s' changes in the modeling. Concerning the limitations of the method, Franceschini et al. (1998) showed using a MD NIRI approach based on a two-layer model that absorption changes in the lower layer can be correctly determined when the layer thickness is less than ~0.6 cm. In conclusion, the MD fNIRI methodology is a promising approach to reduce the sensitivity of fNIRI signals to the extracerebral compartment (i.e. the components SC3 and SC6). However, the removal of the systemic activity type 1 (i.e. SC2) is not possible using this approach.

Depth resolution by imaging approaches. A further development of the MD methodology is to use more sources and detectors and perform forward and inverse modeling in order to determine spatiotemporal absorption changes. Although more complex mathematical models like the diffusion equation (Patterson et al., 1989) have been applied to model the light propagation in tissue, for the low number of sources and detectors and therefore the low complexity initially used in many fNIRS systems, the MBLL law is well suited. Systems working in time domain (TD) and frequency domain (FD) have traditionally used more complex mathematical frameworks based on derivations of the diffusion equation in complex geometries (Arridge et al., 1992) or even direct derivations of the Boltzmann radiative transfer equation (Klose and Larsen, 2006) to model how light travels through highly scattering tissue. These models allow calculating not only the optical properties of bulk tissue but also to reconstruct chromophore concentrations in a three-dimensional space. These tomographic images are obtained by defining how light travels through a highly scattering heterogeneous medium using a model based on the above mentioned mathematical frameworks. This is the so-called forward problem and there are various implementations using methods of different complexity. Once the forward problem is defined it needs to be inverted in order to reconstruct the chromophore concentrations from a given measurement. This is a non-trivial problem which is ill-posed due to the absorbing nature of tissue and the limited amount of light that can be obtained with present setups. For this reason such problems require regularization techniques such as Tikhonov (Tikhonov and Arsenin, 1977) in order to obtain a converging solution.

Numerical methods based on the local solution of the diffusion equation in a meshed space (Arridge et al., 1993; Dehghani et al., 2009a) such as finite elements method (FEM) have been among the most popular methods to define the forward model due to their inherent flexibility to model irregular spaces and the ability to include prior information from other tomographic sources. Linearized solutions of the analytical solution of the diffusion equation (Kak and Slaney, 1988; O'Leary, 1996) have been widely used to model heterogeneous highly scattering tissue due to its relatively simple implementation and its computational efficiency. This last method presented major difficulties when employed for irregular volumes, however this problem has been solved (Ripoll and Ntziachristos, 2006). Monte Carlo methods have been applied as well (Hayakawa et al., 2001) and became very attractive with the advent of GPU based computation (Fang and Boas, 2009), which allowed for parallel simulation of many photons using a desktop PC.

Signal analysis methods to extract the functional brain activity. Besides the technical approaches (like MD or forward/inverse modeling), several signal processing frameworks were developed that use fNIRI signals from different SDS. For example, a class of such approaches

comprises methods based on regression analysis to remove the systemic interferences. Franceschini et al. (2003) placed an fNIRI channel on a non-activated brain region to subtract it from a channel over an activated brain region. This approach is particular, because it not only removes the influence of extracerebral tissue (SC3 and SC6), but also of cerebral (SC4 and SC5) components. Saager and Berger (2005) developed a method of applying a short SDS of 5 mm, which is much less sensitive to deep tissue such as the brain, as a regressor on longer distances and performs a linear regression using a linear minimum mean square estimation (LMMSE) in order to remove the influence of extracerebral layers from the fNIRI signal. This method was successfully tested using fNIRI data from adults (Biallas et al., 2012a; Saager and Berger, 2008; Saager et al., 2011) and newborns (Biallas et al., 2012b; Liao et al., 2010). A similar regression method ('superficial signal regression'), which uses the averages of all short (1.3 cm) SD channels as a regressor, was developed by Gregg et al. (2010). In Saager et al. (2011) an improved version of the approach was presented using an 8-channel probe configuration and 2 small SD channels (5 mm). Gagnon et al. (2011, 2012) investigated how the position of the short SD channel relative to the long SD channel impacts the performance of the method. They concluded that the separation between the channel of interest and the regressor distance should be <1.5 cm. In a further study Gagnon et al. (2014) showed that usage of two short SD channels for the regression analysis is superior to using only one. The short SD channels should be located close to the source of the long SD channel and close to the detector of the same long SD channel. Another finding was that the regression methodology improves the [O_2Hb] signals more than [HHb] signals, which confirms a previous study of the same group (Gagnon et al., 2011). The method of Saager and Berger was further developed by Zhang et al. (2007a) who considered also non-stationarities of the signal by replacing the LMMSE with a least mean squares (LMS) adaptive filtering algorithm. They validated their method using simulated (Zhang et al., 2007a) and real fNIRI data (Zhang et al., 2007b, 2009). An improvement of this method was presented in Y. Zhang et al. (2012) where they described how to use a recursive least squares (RLS) algorithm, which exhibits a fast convergence, instead of the LMS for the adaptive filtering which improves the results. Tian et al. (2011) presented a method that uses two adaptive filters with specific frequency bandwidths to process a reference signal in order to remove it from the target fNIRI signal. As the NIRI-SRS methodology, these approaches reduce the sensitivity of fNIRI to the extracerebral compartment (i.e. the components SC3 and SC6), but they are not able to remove systemic activity type 1 (i.e. SC2).

A further class of approaches is based on state-space modeling using Kalman filtering (Abdelnour and Huppert, 2009; Diamond et al., 2005, 2006; Gagnon et al., 2011, 2014; Kamrani et al., 2012; Kolehmainen et al., 2003; Prince et al., 2003) or recursive least-squares estimation (Aqil et al., 2012a,b). State-space methods model the data as a system with time-varying parameters that have to be estimated. The use of a model-based fNIRI analysis approach by means of the general linear model (GLM) methodology (Bullmore et al., 1996; Friston et al., 1995; Worsley and Friston, 1995) was reported by several authors (e.g. Boas et al., 2003; Çiftçi et al., 2008; Fekete et al., 2011; Hu et al., 2010; Imai et al., 2012; Koh et al., 2007; Moriai-Izawa et al., 2012; Plichta et al., 2007a,b; Schroeter et al., 2004; Tsuzuki et al., 2012; Ye et al., 2009). GLM is a statistical linear model explaining data as a linear combination of an explanatory variable plus an error term. How to combine GLM with a Kalman estimator and to analyze fNIRI data was shown by Hu et al. (2010). Methods using independent component analysis (ICA) (Akgül et al., 2006; Katura et al., 2008; Kohno et al., 2007; Markham et al., 2009; Medvedev et al., 2008; Morren et al., 2004; Schelkanova and Toronov, 2012) or principal component analysis (PCA) (Franceschini et al., 2006; H. Zhang et al., 2010; H. Zhang et al., 2011; Mäki et al., 2010; Sitaram et al., 2007; Soe and Nakagawa, 2008; Virtanen et al., 2012; Y. Zhang et al., 2005) were also developed to address the obstacle of how to remove systemic interferences. Virtanen et al. (2009) compared the ability of ICA and PCA to exclude extracerebral signals and concluded that PCA typically performs equal to or better than ICA. Since they did not use a functional paradigm per se but analyzed hyper- and hypocapnia data, their findings do not automatically apply to fNIRI. According to the findings of Markham et al. (2009), ICA is better suited to extract stimulus-evoked hemodynamic responses. Other approaches presented to reduce the physiological interference and/or remove the influence of the extracerebral compartment from the fNIRI signals include the following: Scarpa et al. (2011) developed a method that first models the physiological interference using a reference channel (with small SDS), and then uses this model for filtering with a non-parametric Bayesian approach. They showed that this method outperforms band-pass- and PCA-based filtering. Heiskala et al. (2012) proposed a Bayesian approximation error approach to reduce the physiological interference. Y. Zhang et al. (2011) presented an advanced signal-regression scheme: an fNIRI channel with a short SDS is decomposed into intrinsic mode functions (IMFs) by using EMD and a weighted sum of these IMFs is used as a regressor to filter out the physiological interference in long SD fNIRI channels. Tanaka et al. (2013) developed a new signal processing method, 'task-related component analysis' (TRCA), to extract task-related components from fNIRI signals by constructing a weighted sum of them while maximizing the covariance or correlation between the task blocks. They showed that the method is able to extract task-related components and also automatically offers the possibility to correct for movement artifacts to a certain degree. This class of methods (state-space modeling, GLM, ICA/PCA, Bayesian filtering with reference, EMD-bases regression, TRCA) is able to remove components SC4–6 and also partially SC3, but are not able to distinguish between SC1 and SC2.

Two other methods (Cui et al., 2010; Yamada et al., 2012) exploit the fact that changes in fNIRI signals have a specific characteristic when caused by functional brain activity or systemic interferences. Specifically, Cui et al. (2010) derived an 'activation signal' that is determined by combining the [O_2Hb] and [HHb] in such a manner that only the anti-correlated parts of the signals remain in the final signal. Yamada et al. (2012) developed a method that separates an fNIRI signal into the neuronal and systemic part by using a system of equations modeling the functional neuronal part ([O_2Hb] and [HHb] are negatively correlated) and the systemic part ([O_2Hb] and [HHb] are positively correlated). The correlation strength is modeled by two parameters where the first parameter can be determined from previous fNIRI experiments and the second parameter is directly determined by using the input fNIRI signals and by minimizing the mutual information between the [O_2Hb] and [HHb] signals. The proposed method gives similar results to the MD fNIRI method developed by Yamada et al. (2009) which is based on the five-layer modeling, the incorporation of μ_s' and μ_a changes and the processing of two fNIRI channels with different SD separations (2 and 3 cm). These two methods (Cui et al., 2010; Yamada et al., 2012) are the only methods of type 1 that enable to reduce the components SC4–5 and, in principle, separating the component SC1 from SC2–3. However, the separability of SC1 from SC2–3 relies on the assumptions made about the characteristic of the systemic interferences. The assumptions used in Cui et al. (2010) and Yamada et al. (2012) work only if the systemic changes are not induced by variations in $PaCO_2$ since in this case the systemic changes have a different characteristic (Scholkmann et al., 2013) compared to the one used for the modeling.

Multivariate methods of type 2

This type of approach is defined as methods that incorporate fNIRI signals and systemic signals (such as BP, skin conductance (SC), heart rate, $P_{ET}CO_2$, etc.) in parallel into the signal analysis in order to distinguish the different fNIRI signal components. Up to now, only a few methods were presented and evaluated that address this task. As an early approach, Morren et al. (2004) used a pulse oximeter placed on

the finger to record the heartbeat waveform which was used as a reference signal in an adaptive filter to remove the component from the fNIRI signals. Obviously, this approach is only able to partly remove systemic activity types 3 (SC5) and 4 (SC6) (i.e. only the heartbeat). Tachtsidis et al. (2010) presented an approach designed to combine fNIRI data with systemic physiological data (i.e. mean blood pressure (MBP), heart rate (HR), and scalp blood flux) in order to separate between the different signal components. They used a GLM for the regression analysis and 'Statistical Parametric Mapping' (SPM) for the statistical group analysis. Another approach combining fNIRI data and systemic physiological signals was presented by Kirilina et al. (2012) who used a GLM model that included a cerebral predictor modeling responses to the experimental task and an additional extracranial predictor to model task-evoked scalp hemodynamic changes which were directly measured in the cutaneous veins using fMRI. They suggest that in particular [O_2Hb] is contaminated by systemic interferences. Patel et al. (2011) presented a method that first decomposes the fNIRI signals using ICA and then performs a correlation analysis with systemic physiological signals (HR, BF and SBF).

In conclusion, as far as we know, the approaches of Kirilina et al. (2012), Patel et al. (2011) and Tachtsidis et al. (2010) are the only ones enabling to separate all components (SC1–6).

fNIRI software

Over the years the complexity of CW fNIRI systems has grown to such extent that nowadays they use the same complex mathematical models as TD-NIRI and FD-NIRI systems to obtain tomographic images. Proprietary reconstruction systems as well as many different open source software products implementing some of the previously described techniques (Arridge et al., 1993; Dehghani et al., 2009b; Fang and Boas, 2009) are available to evaluate the results obtained from NIRI systems. In the following we shortly describe the most important ones.

- HomER2 (PMILab, 2012) is further development of the original version HomER (Huppert et al., 2009). It is a software for studying evoked hemodynamic changes within the brain using fNIRI.
- NIRS-SPM (NIRS-SPM, 2013) is a software package for statistical analysis of fNIRI data using a framework based on a general linear model (GLM) and Sun's tube formula/Lipschitz–Killing curvature (LKC) based expected Euler characteristics.
- fOSA-SPM (fOSA-SPM, 2013) enables the processing and analysis of fNIRI data by using the SPM approach.
- TOAST (TOAST, 2013) is an open-source software that has been developed by the University College London for many years. It was one of the first tools that allowed FEM based image reconstructions of NIRI data including prior anatomical information using time-resolved measurements with different wavelengths. It includes several regularization methods and inverse problem solvers.
- NIRFAST (NIRFAST, 2013) is probably one of the most complete and popular softwares used in the NIRI community. It is a FEM based tool very similar to TOAST (time-resolved measurements are supported, multi wavelength capable, etc.) that allows as well the image reconstruction of fluorescence measurements.
- Photon Migration Imaging Toolbox (PMI) (PMI, 2013) is a software that uses linearized solutions of the diffusion equation to simulate and reconstruct images of NIRI data. It cannot include anatomical information and is restricted to a few standard geometries (infinite medium, semi-infinite medium …).
- Monte Carlo eXtreme (Monte Carlo eXtreme, 2013) is a Monte Carlo simulation platform for NIR light propagation in highly scattering media. It uses Graphics Processing Units (GPU) acceleration to parallelize the simulation of the photons. This tool simulates the forward problem in a more accurate manner than the other methods. Its results can be later used in any of the previously presented tools, to assess the performance of the inversion solver.
- NIRSOFT is a stand-alone software package designed to process, analyze and visualize fNIRI data.
- NAP (Fekete et al., 2011) is a software for noise reduction and statistical inference of fNIRI data.
- POTATo (POTATo, 2013) is a software package for fNIRS signal processing and analysis, developed by Hitachi, Ltd.
- NAVI (NAVI, 2013) is proprietary software developed by NIRx. This software is a FEM based solution that allows the inclusion of prior anatomical data as well as the integration of data coming from other instrumentation such as EEG.
- A collection of different MATLAB functions for fNIRS data processing is available from the website of the Functional Brain Science Lab., Jichi Medical University, Tochigi, Japan (Jichi Medical University, 2013).

Future directions of fNIRI

As one can see in the exponential growth of the number of publications on fNIRI, the development of fNIRI is continuing and much progress has already been made during the last 35 years. It is foreseeable that this progress will be sustained, because the potential of fNIRI is still far from being fully exploited.

For continuous wave fNIRI instrumentation, there will be an incentive to build instruments that incorporate an increased number of light sources and detectors in order to take more advantage of already existing imaging algorithms. These instruments will also offer a higher dynamic range in order to measure at a wider range of SD distances, which will further optimize the depth resolution of the images.

For frequency domain fNIRI, there is already an fNIRI instrument commercially available, which incorporates mature technology at a price comparable to continuous wave instruments. This enables a more accurate quantification of the signals compared to continuous wave instruments. The development in frequency domain will focus on solid state devices with a higher number of detectors, which will be able to measure phase in addition to intensity. For frequency domain as well as for continuous wave and time domain fNIRI instrumentation there will be a trend to increase the number of detectors rather than the number of light sources, because this increases the amount of obtainable information without increasing the energy that is emitted into the tissue. The advantage of frequency domain fNIRI is that it can easily be miniaturized.

Time domain fNIRI will probably experience the largest progress among the three technologies. So far this instrumentation has been bulky and expensive. Novel detectors are being developed, such as e.g. silicon photomultipliers, which are based on single photon avalanche photodiodes (SPADs) (Zimmermann et al., 2013a). So far the silicon photomultipliers are only used in continuous wave instrumentation. But novel technology enables to incorporate time to digital converters (TDCs), which measure the arrival times of photons with a high time resolution in the order of picoseconds. SPADs and TDCs have the advantage that they can be highly miniaturized using standard technology, which leads to camera chips incorporating a high number of detectors, each with the capability to detect single photons and measure their time of flight (Mata Pavia et al., 2011). In addition, picosecond pulsed light sources are becoming more readily available, even supercontinuum light sources with freely selectable wavelengths. Compared to continuous wave and frequency domain fNIRI, time domain fNIRI yields the highest amount of information about the migration of the photons through the tissue. Therefore, it also promises to provide the images with the highest spatial resolution in 3D.

Consequently, in the future, imaging instrumentation will be increasingly sophisticated and fNIRI imaging of the brain will provide an increasing spatial and temporal resolution. This will enable further progress in data analysis algorithms and enhance the range of applications.

fNIRI can easily be combined with other neuroimaging modalities such as fMRI, EEG, PET and MEG, which can also be seen from the number of publications on multimodal imaging systems and their increasing

applications. Combining neuroimaging modalities has the advantage of delivering more comprehensive information, e.g. how electrophysiological and hemodynamic/metabolic signals are correlated.

It is also foreseeable that there will be much progress in probe design. One challenge is to incorporate an increasing number of sources and in particular detectors in the probe and at the same time optimize the ease of application and comfort for the subjects/patient. Another challenge is to minimize the impact of the light absorbing hair. Although these may appear as minor issues, they are important, because the applicability and also the signal quality of fNIRI also depend significantly on them. There are several possible approaches to improve the conditions, e.g. probes can be miniaturized and of less weight. A solution to minimize the effect of hair might be the use of brush optodes (Khan et al., 2012). The coupling of the fibers can be improved e.g. by bio-compatible glue. Another option may lay in wearable photonics textiles (Rothmaier et al., 2008) or electronics (Zysset et al., 2013). Such developments in combination with miniaturized, wireless fNIRI instrumentation will enable unobtrusive measurements in many everyday situations.

There will also be a tremendous development of signal processing for fNIRI. The future will provide fNIRI instrumentation, which will yield orders of magnitude more information than today. This requires algorithms and tools that allow to take advantage of this development and to extract the most relevant results with higher accuracy. At the same time these algorithms need to be efficient enough to calculate these results fast.

An important future task will be the optimization and validation of the methods presented in Methods to separate different components in fNIRI signals section. One promising development already is the combination of the described univariate methods with the multivariate methods 1 and 2. The further development of this approach will be an important topic of research. Regarding the complexity of fNIRI signals with respect to their origin, a proper separation of the fNIRI components is relevant for a correct interpretation of hemodynamic changes, i.e. the separation of the systemic and functional, extra-cerebral and cerebral components. Especially, in combination with imaging in 3D, these methods will become much more powerful and a correct separation of the signal components will lead to more reliable data and thus tremendously facilitate the interpretation of the fNIRI signals. It is obvious that this will be a key factor, which will promote the application fNIRI.

In the future the scope of applications of fNIRI will continuously grow, and probably at increasing speed. The strengths of fNIRI compared to other non-invasive neuroimaging techniques such as EEG, fMRI or MEG include its portability, potential wearability, ease of application, and the low purchase and operation costs (especially when compared to fMRI and MEG), the spatially localized nature of fNIRI in contrast to EEG and the more complete information (O_2Hb in addition to HHb) compared to fMRI and its compatibility with other neuroscience techniques.

Since fNIRI is highly sensitive to hemodynamic fluctuations and oscillations, future studies will exploit this opportunity by gaining deeper insights into the interplay between neuronal and systemic oscillations and the physiological basis of the resting state networks, as already shown (Tong et al., 2013).

In medical diagnostic applications, decisions have to be made for each patient individually. The instrumental and signal analysis developments in fNIRI will lead to more robust and reliable measurements. This will enable reproducible measurements in single subjects. Once this has been achieved, many clinical diagnostic applications will become feasible. Unique possibilities range from early diagnosis of cognitive or motor dysfunctions in preterm infants, which potentially enable early treatment while the brain still has high plasticity, the analysis of brain functions in unconscious intensive care patients, the analysis of the brain state during surgery, the detection of a stroke in the ambulance up to psychiatric applications such as e.g. assessing the state of a disorder, monitoring therapy and the evaluation of brain function in small children to detect and treat functional deficits, etc.

Potentially very important, is the fact that fNIRI is in principle easy to apply, that with continued development, in the future professional staff will not be always necessary. Since fNIRI can be miniaturized and made wearable, this offers new fields of application, for instance as a tool to provide novel forms of therapy for severely impaired stroke patients (Zimmermann et al., 2013b), which will lead to a more effective rehabilitation. It can also be applied as method to provide neuro-feedback for basic neuroscientific studies and/or therapeutic interventions (Sulzer et al., 2013; Tinius and Pa, 2005).

The ability to measure brain activity without being constrained by cables also offers studying novel paradigms, such as hyperscanning, i.e. the analysis of the interaction of brain activity between subjects through measuring simultaneously in two or more subjects (Dommer et al., 2012; Holper et al., 2012, 2013). Studies can be conducted in freely moving subjects. This can be important in sports science, but it is also relevant e.g. in the field of animal welfare, where e.g. the emotional state of sheep (Muehlemann et al., 2011) or goats (Gygax et al., 2013) can be accessed.

It is likely that the development will achieve such high reliability of fNIRI signals that single trial classification can be obtained with a high accuracy. This means that even a single brain activation can be detected. This opens a new field in brain computer interface, which will lead to many everyday life applications. One important application will be prosthetics for stroke victims, paraplegics and other disabled persons, who may be able to guide support systems with their brain activity.

Evidently this enumeration is by no means complete, but it is obvious that today we have merely reached the tip of an iceberg. fNIRI will become an indispensable clinical method and also enter our daily lives.

Conclusions

fNIRI celebrates its 35th birthday. From the single-location measurements at the beginning the instrumentation has developed into first two dimension (topography) and then three dimensions (tomography). Also the methods of analysis have changed tremendously, from the simple modified Beer-Lambert law to sophisticated image reconstruction and data analysis methods. Due to these advances, fNIRI has become a modality that is widely used in neuroscience research and a number of manufacturers provide commercial instrumentation. It is foreseeable that fNIRI will become a clinical tool in the future, which will enable diagnosis in single subjects.

Acknowledgments

We acknowledge funding from the Swiss National Science Foundation, Nano-Tera, CHIRP1 ETH Research Grant CH1-02 09-3, and the Clinical Research Priority Programs Tumor Oxygenation and Molecular Imaging. FS would like to thank Dr. Ilias Tachtsidis (University College London, UK) for fruitful discussion about fNIRI signal processing matters.

Conflict of interest statement

We declare that we have no conflict of interest.

References

Abdelnour, A.F., Huppert, T., 2009. Real-time imaging of human brain function by near-infrared spectroscopy using an adaptive general linear model. Neuroimage 46 (1), 133–143.

Akgül, C.B., Akin, A., Sankur, B., 2006. Extraction of cognitive activity-related waveforms from functional near-infrared spectroscopy signals. Med. Biol. Eng. Comput. 44 (1), 945–958.

Al-Rawi, P.G., Smielewski, P., Kirkpatrick, P.J., 2001. Evaluation of a near-infrared spectrometer (NIRO 300) for the detection of intracranial oxygenation changes in the adult head. Stroke 32 (11), 2492–2500.

Aqil, M., Hong, K.S., Jeong, M.Y., et al., 2012a. Cortical brain imaging by adaptive filtering of NIRS signals. Neuroimage 514 (1), 35–41.

Aqil, M., Hong, K.S., Jeong, M.Y., et al., 2012b. Detection of event-related hemodynamic response to neuroactivation by dynamic modeling of brain activity. Neuroimage 63 (1), 553–568.

Arridge, S.R., Cope, M., Delpy, D.T., 1992. The theoretical basis for the determination of optical pathlengths in tissue: temporal and frequency analysis. Phys. Med. Biol. 37 (7), 1531–1560.

Arridge, S.R., Schweiger, M., Hiraoka, M., et al., 1993. A finite element approach for modeling photon transport in tissue. Med. Phys. 20 (2 Pt 1), 299–309.

Artinis, The Netherlands. www.artinis.com (Last Visited: 01/30/2013).

Atsumori, H., Kiguchi, M., Obata, A., et al., 2009. Development of wearable optical topography system for mapping the prefrontal cortex activation. Rev. Sci. Instrum. 80 (4).

Beer, A., 1852. Bestimmung der Absorption des rothen Lichts in farbigen Flüssigkeiten. Ann. Phys. Chem. 86, 78–88.

Benni, P.B., Chen, B., Dykes, F.D., et al., 2005. Validation of the CAS neonatal NIRS system by monitoring vv-ECMO patients: preliminary results. Adv. Exp. Med. Biol. 566, 195–201.

Biallas, M., Trajkovic, I., Haensse, D., et al., 2012a. Reproducibility and sensitivity of detecting brain activity by simultaneous electroencephalography and near-infrared spectroscopy. Exp. Brain Res. 222 (3), 255–264.

Biallas, M., Trajkovic, I., Hagmann, C., et al., 2012b. Multimodal recording of brain activity in term newborns during photic stimulation by near-infrared spectroscopy and electroencephalography. J. Biomed. Opt. 17 (8), 86011.

Boas, D.A., Gaudette, T., Strangman, G., et al., 2001. The accuracy of near infrared spectroscopy and imaging during focal changes in cerebral hemodynamics. Neuroimage 13 (1), 76–90.

Boas, D.A., Strangman, G., Culver, J.P., et al., 2003. Can the cerebral metabolic rate of oxygen be estimated with near-infrared spectroscopy? Phys. Med. Biol. 48 (15), 2405–2418.

Boas, D.A., Chen, K., Grebert, D., et al., 2004. Improving the diffuse optical imaging spatial resolution of the cerebral hemodynamic response to brain activation in humans. Opt. Lett. 29 (13), 1506–1508.

Bouguer, P., 1729. Essai d'optique, sur la gradation de la lumiere.Claude Jombert, Paris.

Bozkurt, A., Onaral, B., 2004. Safety assessment of near infrared light emitting diodes for diffuse optical measurements. Biomed. Eng. Online 3 (1), 9.

Bozkurt, A., Rosen, A., Rosen, H., et al., 2005. A portable near infrared spectroscopy system for bedside monitoring of newborn brain. Biomed. Eng. Online 4 (1), 29.

Bright, R., 1831. Diseases of the brain and nervous system. Reports of Medical Cases Selected With a View of Illustrating the Symptoms and Care of Diseases by a Reference to Morbid Anatomy, 2, pp. 431–435.

Bullmore, E., Brammer, M., Williams, S.C., et al., 1996. Statistical methods of estimation and inference for functional MR image analysis. Magn. Reson. Med. 35 (2), 261–277.

Buxton, R.B., 2012. Dynamic models of BOLD contrast. Neuroimage 62 (2), 953–961.

Canova, D., Rosatta, S., Basonne, D., et al., 2011. Inconsistent detection of changes in cerebral blood volume by near infrared spectroscopy in standard clinical tests. J. Appl. Physiol. 110 (6), 1646–1655.

Chance, B., Zhuang, Z., UnAh, C., et al., 1993. Cognition-activated low-frequency modulation of light absorption in human brain. Proc. Natl. Acad. Sci. USA 90 (8), 3770–3774.

Cheng, R., Shang, Y., Hayes, D.J., et al., 2012. Noninvasive optical evaluation of spontaneous low frequency oscillations in cerebral hemodynamics. Neuroimage 62 (3), 1445–1454.

Choi, J., Wolf, M., Toronov, V., et al., 2004. Noninvasive determination of the optical properties of adult brain: near-infrared spectroscopy approach. J. Biomed. Opt. 9 (1), 221–229.

Çiftçi, K., Sankur, B., Kahya, Y.P., et al., 2008. Constraining the general linear model for sensible hemodynamic response function waveforms. Med. Biol. Eng. Comput. 46 (8), 779–787.

Cope, M., Delpy, D.T., Wray, S., et al., 1989. A CCD spectrophotometer to quantitate the concentration of chromophores in living tissue utilising the absorption peak of water at 975 nm. Adv. Exp. Med. Biol. 248, 33–40.

Corlu, A., Durduran, T., Choe, R., et al., 2003. Uniqueness and wavelength optimization in continuous-wave multispectral diffuse optical tomography. Opt. Lett. 28 (23), 2339–2341.

Corlu, A., Choe, R., Durduran, T., et al., 2005. Diffuse optical tomography with spectral constraints and wavelength optimization. Appl. Opt. 44 (11), 2082–2093.

Correia, T., Gibson, A., Hebden, J., 2010. Identification of the optimal wavelengths for optical topography: a photon measurement density function analysis. J. Biomed. Opt. 15 (5), 056002.

Cui, X., Bray, S., Reiss, A.L., 2010. Functional near infrared spectroscopy (NIRS) signal improvement based on negative correlation between oxygenated and deoxygenated hemoglobin dynamics. Neuroimage 49 (4), 3039–3046.

Culver, J.P., Ntziachristos, V., Holboke, M.J., et al., 2001. Optimization of optode arrangements for diffuse optical tomography: a singular-value analysis. Opt. Lett. 26 (10), 701–703.

Curling, T.B., 1856. A Practical Treatise on the Diseases of the Testis, and of the Spermatic Cord and Scrotum.Blanchard and Lea, Philadelphia (http://archive.org/details/101504825.nlm.nih.gov).

Cutler, M., 1929. Transillumination as an aid in the diagnosis of breast lesions. Surg. Gynecol. Obstet. 48, 721–729.

Davie, S.N., Grocott, H.P., 2012. Impact of extracranial contamination on regional cerebral oxygen saturation: a comparison of three cerebral oximetry technologies. Anesthesiology 116 (4), 834–840.

Dehghani, H., Eames, M.E., Yalavarthy, P.K., et al., 2009a. Near infrared optical tomography using NIRFAST: algorithm for numerical model and image reconstruction. Commun. Numer. Methods Eng. 25 (6), 711–732.

Dehghani, H., White, B.R., Zeff, B.W., et al., 2009b. Depth sensitivity and image reconstruction analysis of dense imaging arrays for mapping brain function with diffuse optical tomography. Appl. Opt. 48 (10), D137–D143.

Delpy, D.T., Cope, M., van der Zee, P., et al., 1988. Estimation of optical pathlength through tissue from direct time of flight measurement. Phys. Med. Biol. 33 (12), 1433–1442.

Devor, A., Boas, D.A., Einevoll, G.T., et al., 2012. Neuronal basis of non-invasive functional imaging: from microscopic neurovascular dynamics to BOLD fMRI. Adv. Neurobiol. 4 (433–500).

Diamond, S.G., Huppert, T.J., Kolehmainen, V., et al., 2005. Physiological system identification with the Kalman filter in diffuse optical tomography. Med. Image Comput. Comput. Assist. Interv. 8 (2), 649–656.

Diamond, S.G., Huppert, T.J., Kolehmainen, V., et al., 2006. Dynamic physiological modeling for functional diffuse optical tomography. Neuroimage 30 (1), 88–101.

Diehl, R.R., Linden, D., Lücke, D., et al., 1995. Phase relationship between cerebral blood flow velocity and blood pressure. A clinical test of autoregulation. Stroke 26 (10), 1801–1804.

Diop, M., Elliott, J.T., Tichauer, K.M., et al., 2009. A broadband continuous-wave multichannel near-infrared system for measuring regional cerebral blood flow and oxygen consumption in newborn piglets. Rev. Sci. Instrum. 80 (5), 054302.

Dommer, L., Jager, N., Scholkmann, F., et al., 2012. Between-brain coherence during joint n-back task performance: a two-person functional near-infrared spectroscopy study. Behav. Brain Res. 234 (2), 212–222.

Droste, D.W., Krauss, J.K., 1997. Oscillations of cerebrospinal fluid pressure in nonhydrocephalic persons. Neurol. Res. 19 (2), 135–138.

Drummond, P.D., 1999. Facial flushing during provocation in women. Psychophysiology 36 (3), 325–332.

Drummond, P.D., Lance, J.W., 1987. Facial flushing and sweating mediated by the sympathetic nervous system. Brain 110 (3), 793–803.

Duncan, A., Meek, J.H., Clemence, M., et al., 1995. Optical pathlength measurements on adult head, calf and forearm and the head of the newborn infant using phase resolved optical spectroscopy. Phys. Med. Biol. 40 (2), 295–304.

Duncan, A., Meek, J.H., Clemence, M., et al., 1996. Measurement of cranial optical path length as a function of age using phase resolved near infrared spectroscopy. Pediatr. Res. 39 (5), 889–894.

Durduran, T., Choe, R., Baker, W.B., et al., 2010. Diffuse optics for tissue monitoring and tomography. Rep. Prog. Phys. 73 (7), 076701.

Eames, M.E., Wang, J., Pogue, B.W., et al., 2008. Wavelength band optimization in spectral near-infrared optical tomography improves accuracy while reducing data acquisition and computational burden. J. Biomed. Opt. 13 (5), 054037.

Edwards, A.D., Wyatt, J.S., Richardson, C., et al., 1988. Cotside measurement of cerebral blood flow in ill newborn infants by near infrared spectroscopy. Lancet 2 (8614), 770–771.

Ellis, H., 2012. Anatomy of head injury. Surgery 30 (3), 99–101.

Enzmann, D.R., Pelc, N.J., 1992. Brain motion: measurement with phase-contrast MR imaging. Radiology 185 (3), 653–660.

Essenpreis, M., Elwell, C.E., Cope, M., et al., 1993. Spectral dependence of temporal point spread functions in human tissues. Appl. Opt. 32 (4), 418–425.

Everdell, N.L., Gibson, A.P., Tullis, I.D.C., et al., 2005. A frequency multiplexed near-infrared topography system for imaging functional activation in the brain. Rev. Sci. Instrum. 76 (9).

Fabbri, F., Sassaroli, A., Henry, M.E., et al., 2004. Optical measurements of absorption changes in two-layered diffusive media. Phys. Med. Biol. 49 (7), 1183–1201.

Fang, Q., Boas, D.A., 2009. Monte Carlo simulation of photon migration in 3D turbid media accelerated by graphics processing units. Opt. Express 17 (22), 20178–20190.

Fantini, S., Franceschini, M.A., Gratton, E., 1994. Semi-infinite-geometry boundary-problem for light migration in highly scattering media — a frequency-domain study in the diffusion-approximation. J. Opt. Soc. Am. B Opt. Phys. 11 (10), 2128–2138.

Feinberg, D.A., Mark, A.S., 1987. Human brain motion and cerebrospinal fluid circulation demonstrated with MR velocity imaging. Radiology 163 (3), 793–799.

Fekete, T., Rubin, D., Carlson, J.M., et al., 2011. The NIRS analysis package: noise reduction and statistical inference. PLoS One 6 (9), e24322.

Ferrari, M., Quaresima, V., 2012. A brief review on the history of human functional near-infrared spectroscopy (fNIRS) development and fields of application. Neuroimage 63 (2), 921–935.

Ferrari, M., Mottola, L., Quaresima, V., 2004. Principles, techniques, and limitations of near infrared spectroscopy. Can. J. Appl. Physiol. 29 (4), 463–487.

Flexman, M.L., Kim, H.K., Stoll, R., et al., 2012. A wireless handheld probe with spectrally constrained evolution strategies for diffuse optical imaging of tissue. Rev. Sci. Instrum. 83 (3), 033108.

fNIR Devices, USA. [www.fnirdevices.com/www.biopac.com]. Last visited: 01/30/2013.

fOSA-SPM, 2013. Website http://www.medphys.ucl.ac.uk/research/nirs/software_fosa.html (Last Visited: 01/30/2013).

Franceschini, M.A., Fantini, S., Paunescu, L.A., et al., 1998. Influence of a superficial layer in the quantitative spectroscopic study of strongly scattering media. Appl. Opt. 37 (31), 7447–7458.

Franceschini, M.A., Fantini, S., Thompson, J.H., et al., 2003. Hemodynamic evoked response of the sensorimotor cortex measured noninvasively with near-infrared optical imaging. Psychophysiology 40 (4), 548–560.

Franceschini, M.A., Joseph, D.K., Huppert, T.J., et al., 2006. Diffuse optical imaging of the whole head. J. Biomed. Opt. 11 (5), 054007.

Friese, S., Hamhaber, U., Erb, M., et al., 2004. The influence of pulse and respiration on spinal cerebrospinal fluid pulsation. Invest. Radiol. 39 (2), 120–130.

Friston, K.J., Holmes, A.P., Worsley, K.J., et al., 1995. Statistical parametric maps in functional imaging: a general linear approach. Hum. Brain Mapp. 2 (4), 189–210.

Funane, T., Atsumori, H., Sato, H., et al., 2009. Relationship between wavelength combination and signal-to-noise ratio in measuring hemoglobin concentrations using visible or near-infrared light. Opt. Rev. 16 (4), 442–448.
Gagnon, L., Perdue, K., Greve, D.N., et al., 2011. Improved recovery of the hemodynamic response in diffuse optical imaging using short optode separations and state-space modeling. Neuroimage 56 (3), 1362–1371.
Gagnon, L., Cooper, R.J., Yucel, M.A., et al., 2012. Short separation channel location impacts the performance of short channel regression in NIRS. Neuroimage 59 (3), 2518–2528.
Gagnon, L., Yücel, M.A., Boas, D.A., et al., 2014. Further improvement in reducing superficial contamination in NIRS using double short separation measurements. Neuroimage 85, 127–135.
Giacometti, P., Diamond, S.G., 2013. Diffuse optical tomography for brain imaging: continuous wave instrumentation and linear analysis methods. Optical Methods and Instrumentation in Brain Imaging and Therapy, 3, pp. 57–85.
Gibson, A.P., Hebden, J.C., Arridge, S.R., 2005. Recent advances in diffuse optical imaging. Phys. Med. Biol. 50 (4), R1–R43.
Giller, C.A., Giller, A.M., Cooper, C.R., et al., 2000. Evaluation of the cerebral hemodynamic response to rhythmic handgrip. J. Appl. Physiol. 88 (6), 2205–2213.
Goadsby, P.J., Knight, Y.E., Hoskin, K.L., et al., 1997. Stimulation of an intracranial trigeminally-innervated structure selectively increases cerebral blood flow. Brain Res. 751 (2), 247–252.
Gratton, G., Corballis, P.M., 1995. Removing the heart from the brain: compensation for the pulse artifact in the photon migration signal. Psychophysiology 32 (3), 292–299.
Gregg, N.M., White, B.R., Zeff, B.W., et al., 2010. Brain specificity of diffuse optical imaging: improvements from superficial signal regression and tomography. Front. Neuroenerg. 2 (14), 1–8.
Greicius, M.D., Supekar, K., Menon, V., et al., 2009. Resting-state functional connectivity reflects structural connectivity in the default mode network. Cereb. Cortex 19 (1), 72–78.
Gupta, S., Soellinger, M., Grzybowski, D.M., et al., 2010. Cerebrospinal fluid dynamics in the human cranial subarachnoid space: an overlooked mediator of cerebral disease. I. Computational model. J. R. Soc. Interface 7 (49), 1195–1204.
Gygax, L., Reefmann, N., Wolf, M., et al., 2013. Prefrontal cortex activity, sympathovagal reaction and behaviour distinguish between situations of feed reward and frustration in dwarf goats. Behav. Brain Res. 239, 104–114.
Habermehl, C., Holtze, S., Steinbrink, J., et al., 2012a. Somatosensory activation of two fingers can be discriminated with ultrahigh-density diffuse optical tomography. Neuroimage 59 (4), 3201–3211.
Habermehl, C., Schmitz, C., Koch, S.P., et al., 2012b. Investigating hemodynamics in scalp and brain using high-resolution diffuse optical tomography in humans. Biomedical Optics — Brain Imaging. BSu2A.2.
Haeussinger, F.B., Heinzel, S., Hahn, T., et al., 2011. Simulation of near-infrared light absorption considering individual head and prefrontal cortex anatomy: implications for optical neuroimaging. PLoS One 6 (10), e26377.
Hamel, E., 2006. Perivascular nerves and the regulation of cerebrovascular tone. J. Appl. Physiol. 100 (3), 1059–1064.
Hayakawa, C.K., Spanier, J., Bevilacqua, F., et al., 2001. Perturbation monte carlo methods to solve inverse photon migration problems in heterogeneous tissues. Opt. Lett. 26 (17), 1335–1337.
Hazeki, O., Tamura, M., 1989. Near infrared quadruple wavelength spectrophotometry of the rat head. Adv. Exp. Med. Biol. 248, 63–69.
Hebden, J.C., Cooper, R.J., Gibson, A., et al., 2012. Simultaneous EEG and diffuse optical imaging of seizure-related hemodynamic activity in the newborn infant brain. Biophotonics: Photonic Solutions for Better Health Care III: Proc. SPIE, 8427, p. 84271N-6.
Heiskala, J., Kolehmainen, V., Tarvainen, T., et al., 2012. Approximation error method can reduce artifacts due to scalp blood flow in optical brain activation imaging. J. Biomed. Opt. 17 (9), 096012.
Hiraoka, M., Firbank, M., Essenpreis, M., et al., 1993. A monte carlo investigation of optical pathlength in inhomogeneous tissue and its application to near-infrared spectroscopy. Phys. Med. Biol. 38 (12), 1859–1876.
Hitachi, Japan. www.hitachimed.com (Last Visited: 01/30/2013).
Holper, L., Scholkmann, F., Wolf, M., 2012. Between-brain connectivity during imitation measured by fNIRS. Neuroimage 63 (1), 212–222.
Holper, L., Goldin, A.P., Shalóm, D.E., et al., 2013. The teaching and the learning brain: a cortical hemodynamic marker of teacher–student interactions in the Socratic dialog. Int. J. Educ. Res. 59, 1–10.
Hoshi, Y., 2003. Functional near-infrared optical imaging: utility and limitations in human brain mapping. Psychophysiology 40 (4), 511–520.
Hoshi, Y., Tamura, M., 1993. Detection of dynamic changes in cerebral oxygenation coupled to neuronal function during mental work in man. Neurosci. Lett. 150 (1), 5–8.
Hoshi, Y., Hazeki, O., Kakihana, Y., et al., 1997. Redox behavior of cytochrome oxidase in the rat brain measured by near-infrared spectroscopy. J. Appl. Physiol. 83 (6), 1842–1848.
Hoshi, Y., Kosaka, S., Xie, Y., et al., 1998. Relationship between fluctuations in the cerebral hemoglobin oxygenation state and neuronal activity under resting conditions in man. Neurosci. Lett. 245 (3), 147–150.
Hu, X.S., Hong, K.S., Ge, S.S., et al., 2010. Kalman estimator- and general linear model-based on-line brain activation mapping by near-infrared spectroscopy. Biomed. Eng. Online 9, 82.
Hueber, D.M., Fantini, S., Cerussi, A.E., et al., 1999. New optical probe designs for absolute (self-calibrating) NIR tissue hemoglobin measurements. Optical Tomography and Spectroscopy of Tissue III: Proc. SPIE, 3597, pp. 618–631.
Hüfner, G., 1894. Neue Versuche zur Bestimmung der Sauerstoffcapacität des Blutfarbstoffs. Arch. Pathol. Anat. Physiol. Klin. Med. 55, 130–176.
Huppert, T.J., Diamond, S.G., Franceschini, M.A., et al., 2009. Homer: a review of time-series analysis methods for near-infrared spectroscopy of the brain. Appl. Opt. 48 (10), D280–D298.
Imai, T., Sato, T., Nambo, I., et al., 2012. Estimating brain activity of motor learning by using fNIRS-GLM analysis. Neural Inf. Process. 7663, 401–408.
International Commission on Non-Ionizing Radiation Protection, 1997. Guidelines on limits of exposure to broad-band incoherent optical radiation (0.38 to 3 μm). Health Phys. 73 (3), 539–554.
International Commission on Non-Ionizing Radiation Protection, 2000. Revision of the guidelines on limits of exposure to laser radiation of wavelengths between 400 nm and 1.4 μm. Health Phys. 79 (4), 431–440.
ISS, USA. www.iss.com (Last Visited: 01/30/2013).
Ito, Y., Kennan, R.P., Watanabe, E., et al., 2000. Assessment of heating effects in skin during continuous wave near infrared spectroscopy. J. Biomed. Opt. 5 (4), 383–390.
Izzetoglu, M., Devaraj, A., Bunce, S., et al., 2005. Motion artifact cancellation in NIR spectroscopy using Wiener filtering. IEEE Trans. Biomed. Eng. 52 (5), 934–938.
Janesick, J.R., 2001. Scientific Charge-Coupled Devices.SPIE Press, Bellingham, WA (http://ebooks.spiedigitallibrary.org/book.aspx?bookid=174).
Jang, K.E., Tak, S., Jung, J., et al., 2009. Wavelet minimum description length detrending for near-infrared spectroscopy. J. Biomed. Opt. 14 (3), 034004.
Jelzow, A., Tachtsidis, I., Kirilina, E., et al., 2011. Simultaneous measurement of time-domain fNIRS and physiological signals during a cognitive task. European Conference on Biomedical Optics: Mapping of Brain Function With DOI and Multimodal Imaging, 808803.
Jichi Medical University, 2013. Website http://www.jichi.ac.jp/brainlab/contact.html (Last Visited: 01/30/2013).
Jobsis, F.F., 1977. Noninvasive, infrared monitoring of cerebral and myocardial oxygen sufficiency and circulatory parameters. Science 198 (4323), 1264–1267.
Joseph, D.K., Huppert, T.J., Franceschini, M.A., et al., 2006. Diffuse optical tomography system to image brain activation with improved spatial resolution and validation with functional magnetic resonance imaging. Appl. Opt. 45 (31), 8142–8151.
Julien, C., 2006. The enigma of Mayer waves: facts and models. Cardiovasc. Res. 70 (1), 12–21.
Kak, A.C., Slaney, M., 1988. Principles of Computerized Tomographic Imaging. IEEE Press, New York.
Kamrani, E., Foroushani, A.N., Vaziripour, M., et al., 2012. Efficient hemodynamic states stimulation using fNIRS data with the extended Kalman filter and bifurcation analysis of balloon model. J. Biomed. Sci. Eng. 5, 609–628.
Kao, Y.H., Guo, W.Y., Liou, A.J., et al., 2008. The respiratory modulation of intracranial cerebrospinal fluid pulsation observed on dynamic echo planar images. Magn. Reson. Imaging 26 (2), 198–205.
Kashyap, D., Chu, N., Apte, A., et al., 2007. Development of broadband multi-channel NIRS (near infrared spectroscopy) imaging system for quantification of spatial distribution of hemoglobin derivatives. Optical Tomography and Spectroscopy of Tissue VII: Proc SPIE, 6434, p. 64341X.
Kato, T., Kamei, A., Takashima, S., et al., 1993. Human visual cortical function during photic stimulation monitoring by means of near-infrared spectroscopy. J. Cereb. Blood Flow Metab. 13 (3), 516–520.
Katura, T., Sato, H., Fuchino, Y., et al., 2008. Extracting task-related activation components from optical topography measurement using independent components analysis. J. Biomed. Opt. 13 (5), 054008.
Kawaguchi, H., Okui, N., Sakaguchi, K., et al., 2008. Theoretical analysis of crosstalk between oxygenated and deoxygenated haemoglobin in focal brain-activation measurements by near-infrared topography. Opto-Electron. Rev. 16 (4), 404–412.
Khan, B., Wildey, C., Francis, R., et al., 2012. Improving optical contact for functional near-infrared brain spectroscopy and imaging with brush optodes. Biomed. Opt. Express 3 (5), 878–898.
Kiguchi, M., Ichikawa, N., Atsumori, H., et al., 2007. Comparison of light intensity on the brain surface due to laser exposure during optical topography and solar irradiation. J. Biomed. Opt. 12 (6), 062108.
Kirilina, E., Jelzow, A., Heine, A., et al., 2012. The physiological origin of task-evoked systemic artefacts in functional near infrared spectroscopy. Neuroimage 61 (1), 70–81.
Klose, A.D., Larsen, E.W., 2006. Light transport in biological tissue based on the simplified spherical harmonics equations. J. Comput. Phys. 220 (1), 441–470.
Kocsis, L., Herman, P., Eke, A., 2006. The modified Beer–Lambert law revisited. Phys. Med. Biol. 51 (5), N91–N98.
Koh, P.H., Glaser, D.E., Flandin, G., et al., 2007. Functional optical signal analysis: a software tool for near-infrared spectroscopy data processing incorporating statistical parametric mapping. J. Biomed. Opt. 12 (6), 064010.
Kohno, S., Miyai, I., Seiyama, A., et al., 2007. Removal of the skin blood flow artifact in functional near-infrared spectroscopic imaging data through independent component analysis. J. Biomed. Opt. 12 (6), 062111.
Kolehmainen, V., Prince, S., Arridge, S.R., et al., 2003. State-estimation approach to the nonstationary optical tomography problem. J. Opt. Soc. Am. A Opt. Image Sci. Vis. 20 (5), 876–889.
Kono, T., Matsuo, K., Tsunashima, K., et al., 2007. Multiple-time replicability of near-infrared spectroscopy recording during prefrontal activation task in healthy men. Neurosci. Res. 57 (4), 504–512.
Kurihara, K., Kikukawa, A., Kobayashi, A., 2003. Cerebral oxygenation monitor during head-up and -down tilt using near-infrared spatially resolved spectroscopy. Clin. Physiol. Funct. Imaging 23 (4), 177–181.
Lambert, J.H., 1760. Photometria sive de mensura et gradibus luminis, colorum et umbrae. Eberhardt Klett, Augsburg.

Leamy, D.J., Ward, T.E., 2010. A novel co-locational and concurrent fNIRS/EEG measurement system: design and initial results. Conf. Proc. IEEE Eng. Med. Biol. Soc. 2010, 4230–4233.
Liao, S.M., Gregg, N.M., White, B.R., et al., 2010. Neonatal hemodynamic response to visual cortex activity: high-density near-infrared spectroscopy study. J. Biomed. Opt. 15 (2), 026010.
Liebert, A., Wabnitz, H., Steinbrink, J., et al., 2004. Time-resolved multidistance near-infrared spectroscopy of the adult head: intracerebral and extracerebral absorption changes from moments of distribution of times of flight of photons. Appl. Opt. 43 (15), 3037–3047.
Lina, J.M., Dehaes, M., Matteau-Pelletier, C., et al., 2008. Complex wavelets applied to diffuse optical spectroscopy for brain activity detection. Opt. Express 16 (2), 1029–1050.
Lina, J.M., Matteau-Pelletier, C., Dehaes, M., et al., 2010. Wavelet-based estimation of the hemodynamic responses in diffuse optical imaging. Med. Image Anal. 14 (4), 606–616.
Liu, J.M., 2005. Photonic Devices.Cambridge University Press, Cambridge.
Maki, A., Yamashita, Y., Ito, Y., et al., 1995. Spatial and temporal analysis of human motor activity using noninvasive NIR topography. Med. Phys. 22 (12), 1997–2005.
Mäki, H., Näsi, T., Kotilahti, K., et al., 2010. Characterizing cerebral and extracerebral components in TMS-evoked near-infrared spectroscopy signals. Advances in Biomagnetism — Biomag 2010 IFMBE Proc. 28, 88–91.
Markham, J., White, B.R., Zeff, B.W., et al., 2009. Blind identification of evoked human brain activity with independent component analysis of optical data. Hum. Brain Mapp. 30 (8), 2382–2392.
Mata Pavia, J.M., Charbon, E., Wolf, M., 2011. 3D near-infrared imaging based on a single-photon avalanche diode array sensor. Diffuse Optical Imaging Iii, p. 8088.
Matcher, S.J., Cope, M., Delpy, D.T., 1994. Use of the water absorption spectrum to quantify tissue chromophore concentration changes in near-infrared spectroscopy. Phys. Med. Biol. 39 (1), 177–196.
Matcher, S.J., Elwell, C.E., Cooper, C.E., et al., 1995a. Performance comparison of several published tissue near-infrared spectroscopy algorithms. Anal. Biochem. 227 (1), 54–68.
Matcher, S.J., Kirkpatrick, P.J., Nahid, K., et al., 1995b. Absolute quantification methods in tissue near-infrared spectroscopy. Proc. SPIE 2389, 486–495.
Matcher, S.J., Cope, M., Delpy, D.T., 1997. In vivo measurements of the wavelength dependence of tissue-scattering coefficients between 760 and 900 nm measured with time-resolved spectroscopy. Appl. Opt. 36 (1), 386–396.
Matsumoto, T., Saito, K., Nakamura, A., et al., 2012. Dried-bonito aroma components enhance salivary hemodynamic responses to broth tastes detected by near-infrared spectroscopy. J. Agric. Food Chem. 60 (3), 805–811.
Matteau-Pelletier, C., Dehaes, M., Lesage, F., et al., 2009. 1/f noise in diffuse optical imaging and wavelet-based response estimation. IEEE Trans. Med. Imaging 28 (3), 415–422.
Matthes, K., Gross, F., 1938a. Fortlaufende Registrierung der Lichtabsorption des Blutes in zwei verschiedenen Spektralbezirken. Naunyn Schmiedebergs Arch. Pharmacol. 191 (2–4), 381–390.
Matthes, K., Gross, F., 1938b. Untersuchung über die Absorption von rotem und ultrarotem Licht durch kohlenoxygesättigstes, sauerstoffgesättigtes und reduziertes Blut. Naunyn Schmiedebergs Arch. Pharmacol. 191 (2–4), 369–380.
Matthes, K., Gross, F., 1938c. Zur Methode der fortlaufenden Registrierung der Farbe des menschlichen Blutes. Naunyn Schmiedebergs Arch. Pharmacol. 191 (2–4), 523–528.
McIntosh, M.A., Shahani, U., Boulton, R.G., et al., 2010. Absolute quantification of oxygenated hemoglobin within the visual cortex with functional near infrared spectroscopy (fNIRS). Invest. Ophthalmol. Vis. Sci. 51 (9), 4856–4860.
Medvedev, A.V., Kainerstorfer, J., Borisov, S.V., et al., 2008. Event-related fast optical signal in a rapid object recognition task: improving detection by the independent component analysis. Brain Res. 1236, 145–158.
Minati, L., Jones, C.L., Gray, M.A., et al., 2009. Emotional modulation of visual cortex activity: a functional near-infrared spectroscopy study. Neuroreport 20 (15), 1344–1350.
Minati, L., Kress, I.U., Visani, E., et al., 2011. Intra- and extra-cranial effects of transient blood pressure changes on brain near-infrared spectroscopy (NIRS) measurements. J. Neurosci. Methods 197 (2), 283–288.
Monte Carlo eXtreme, 2013. Website http://mcx.sourceforge.net/cgi-bin/index.cgi (Last Visited: 01/30/2013).
Moody, M., Panerai, R.B., Eames, P.J., et al., 2005. Cerebral and systemic hemodynamic changes during cognitive and motor activation paradigms. Am. J. Physiol. Regul. Integr. Comp. Physiol. 288 (6), R1581–R1588.
Moriai-Izawa, A., Dan, H., Dan, I., et al., 2012. Multichannel fNIRS assessment of overt and covert confrontation naming. Brain Lang. 121 (3), 185–193.
Morren, G., Wolf, M., Lemmerling, P., et al., 2004. Detection of fast neuronal signals in the motor cortex from functional near infrared spectroscopy measurements using independent component analysis. Med. Biol. Eng. Comput. 42 (1), 92–99.
MRRA, USA. www.mrrainc.com (Last Visited: 01/30/2013).
Muehlemann, T., Haensse, D., Wolf, M., 2008. Wireless miniaturized in-vivo near infrared imaging. Opt. Express 16 (14), 10323–10330.
Muehlemann, T., Reefmann, N., Wechsler, B., et al., 2011. In vivo functional near-infrared spectroscopy measures mood-modulated cerebral responses to a positive emotional stimulus in sheep. Neuroimage 54 (2), 1625–1633.
Muldoon, M.F., Bachen, E.A., Manuck, S.B., et al., 1992. Acute cholesterol responses to mental stress and change in posture. Arch. Intern. Med. 152 (4), 775–780.
Näsi, T., Virtanen, J., Noponen, T., et al., 2011. Spontaneous hemodynamic oscillations during human sleep and sleep stage transitions characterized with near-infrared spectroscopy. PLoS One 6 (10), e25415.
NAVI, 2013. Website http://www.nirx.net/software/navi (Last Visited: 01/30/2013).
Nicolai, L., 1932a. Fortgesetzte Untersuchungen über den Verlauf der Oxyhämoglobinreduktion in der menschlichen Haut. Pflugers Arch. 230 (1), 238–245.
Nicolai, L., 1932b. Über Sichtbarmachung, Verlauf und chemische Kinetik der Oxyhömoglobinreduktion im lebenden Gewebe, besonders in der menschlichen Haut. Pflugers Arch. 229 (1), 372–384.
NIRFAST, 2013. Website http://www.dartmouth.edu/nir/nirfast/ (Last Visited: 01/30/2013).
NIRS-SPM, 2013. Website http://bisp.kaist.ac.kr/NIRS-SPM.html (Last Visited: 01/30/2013).
NIRx, USA. www.nirx.net (Last Visited: 01/30/2013).
O'Leary, M.A., 1996. Imaging With Diffuse Photon Density Waves.University of Pennsylvania (PhD Thesis. [http://www.physics.upenn.edu/yodhlab/theses/maureen_oleary.pdf]).
Obrig, H., Villringer, A., 2003. Beyond the visible-imaging the human brain with light. J. Cereb. Blood Flow Metab. 23 (1), 1–18.
Obrig, H., Neufang, M., Wenzel, R., et al., 2000a. Spontaneous low frequency oscillations of cerebral hemodynamics and metabolism in human adults. Neuroimage 12 (6), 623–639.
Obrig, H., Wenzel, R., Kohl, M., et al., 2000b. Near-infrared spectroscopy: does it function in functional activation studies of the adult brain? Int. J. Psychophysiol. 35 (2–3), 125–142.
Okui, N., Okada, E., 2005. Wavelength dependence of crosstalk in dual-wavelength measurement of oxy- and deoxy-hemoglobin. J. Biomed. Opt. 10 (1), 011015.
Özgören, M., Tetik, M., Izzetoglu, K., et al., 2012. Effect of body position on NIRS based hemodynamic measures from prefrontal cortex. Advances in Brain Inspired Cognitive Systems, 7366, pp. 138–146.
Patel, S., Katura, T., Maki, A., et al., 2011. Quantification of systemic interference in optical topography data during frontal lobe and motor cortex activation: an independent component analysis. Adv. Exp. Med. Biol. 701, 45–51.
Patterson, M.S., Chance, B., Wilson, B.C., 1989. Time resolved reflectance and transmittance for the non-invasive measurement of tissue optical properties. Appl. Opt. 28 (12), 2331–2336.
Payne, S.J., Mohammad, J., Tisdall, M.M., et al., 2011. Effects of arterial blood gas levels on cerebral blood flow and oxygen transport. Biomed. Opt. Express 2 (4), 966–979.
Peng, T., Ainslie, P.N., Cotter, J.D., et al., 2008. The effects of age on the spontaneous low-frequency oscillations in cerebral and systemic cardiovascular dynamics. Physiol. Meas. 29 (9), 1055–1069.
Perutz, M., 1995. Hoppe-Seyler, Stokes and haemoglobin. Biol. Chem. Hoppe Seyler 376 (8), 449–450.
Phillip, D., Schytz, H.W., Selb, J., et al., 2012. Low frequency oscillations in cephalic vessels assessed by near infrared spectroscopy. Eur. J. Clin. Invest. 42 (11), 1180–1188.
Plichta, M.M., Herrmann, M.J., Baehne, C.G., et al., 2006. Event-related functional near-infrared spectroscopy (fNIRS): are the measurements reliable? Neuroimage 31 (1), 116–124.
Plichta, M.M., Heinzel, S., Ehlis, A.C., et al., 2007a. Model-based analysis of rapid event-related functional near-infrared spectroscopy (NIRS) data: a parametric validation study. Neuroimage 35 (2), 625–634.
Plichta, M.M., Herrmann, M.J., Baehne, C.G., et al., 2007b. Event-related functional near-infrared spectroscopy (fNIRS) based on craniocerebral correlations: reproducibility of activation? Hum. Brain Mapp. 28 (8), 733–741.
PMI, 2013. Website http://www.nmr.mgh.harvard.edu/PMI/toolbox/index.html (Last Visited: 01/30/2013).
PMILab, 2012. Homer2. http://www.nmr.mgh.harvard.edu/PMI/resources/homer2/home.htm (Last Visited: 01/24/2013).
Poeppel, T.D., Terborg, C., Hautzel, H., et al., 2007. Cerebral haemodynamics during hypo- and hypercapnia: determination with simultaneous 15o-butanol-pet and transcranial doppler sonography. Nuklearmedizin 46 (3), 93–100.
Poncelet, B.P., Wedeen, V.J., Weisskoff, R.M., et al., 1992. Brain parenchyma motion: measurement with cine echo-planar MR imaging. Radiology 185 (3), 645–651.
POTATo, 2013. Website http://www.hitachi.co.jp/products/ot/study/kaiseki.html (Last Visited: 01/30/2013).
Prince, S., Kolehmainen, V., Kaipio, J.P., et al., 2003. Time-series estimation of biological factors in optical diffusion tomography. Phys. Med. Biol. 48 (11), 1491–1504.
Pringle, J., Roberts, C., Kohl, M., et al., 1999. Near infrared spectroscopy in large animals: optical pathlength and influence of hair covering and epidermal pigmentation. Vet. J. 158 (1), 48–52.
Pucci, O., Toronov, V., St Lawrence, K., 2010. Measurement of the optical properties of a two-layer model of the human head using broadband near-infrared spectroscopy. Appl. Opt. 49 (32), 6324–6332.
Raichle, M.E., 2009. A paradigm shift in functional brain imaging. J. Neurosci. 29 (41), 12729–12734.
Reinhard, M., Wehrle-Wieland, E., Grabiak, D., et al., 2006. Oscillatory cerebral hemodynamics—the macro- vs. microvascular level. J. Neurol. Sci. 250 (1–2), 103–109.
Renker, D., 2007. New trends on photodetectors. Nucl. Inst. Methods Phys. Res. A 571 (1–2), 1–6.
Ripoll, J., Ntziachristos, V., 2006. From finite to infinite volumes: removal of boundaries in diffuse wave imaging. Phys. Rev. Lett. 96 (17).
Rogue Research, Canada. www.rogue-research.com (Last Visited: 01/30/2013).
Rothmaier, M., Selm, B., Spichtig, S., et al., 2008. Photonic textiles for pulse oximetry. Opt. Express 16 (17), 12973–12986.
Saager, R.B., Berger, A.J., 2005. Direct characterization and removal of interfering absorption trends in two-layer turbid media. J. Opt. Soc. Am. A 22 (9), 1874–1882.
Saager, R.B., Berger, A.J., 2008. Measurement of layer-like hemodynamic trends in scalp and cortex: Implications for physiological baseline suppression in functional near-infrared spectroscopy. J. Biomed. Opt. 13 (3), 034017.
Saager, R.B., Telleri, N.L., Berger, A.J., 2011. Two-detector Corrected Near Infrared Spectroscopy (C-NIRS) detects hemodynamic activation responses more robustly than single-detector NIRS. Neuroimage 55 (4), 1679–1685.
Safonova, L.P., Michalos, A., Wolf, U., et al., 2004. Age-correlated changes in cerebral hemodynamics assessed by near-infrared spectroscopy. Arch. Gerontol. Geriatr. 39 (3), 207–225.

Sasai, S., Homae, F., Watanabe, H., et al., 2012. A NIRS-fMRI study of resting state network. Neuroimage 63 (1), 179–193.
Sassaroli, A., Fantini, S., 2004. Comment on the modified Beer–Lambert law for scattering media. Phys. Med. Biol. 49 (14), N255–N257.
Sato, H., Kiguchi, M., Kawaguchi, F., et al., 2004. Practicality of wavelength selection to improve signal-to-noise ratio in near-infrared spectroscopy. Neuroimage 21 (4), 1544–1562.
Sato, H., Obata, A.N., Moda, I., et al., 2011. Application of near-infrared spectroscopy to measurement of hemodynamic signals accompanying stimulated saliva secretion. J. Biomed. Opt. 16 (4), 047002.
Scarpa, F., Cutini, S., Scatturin, P., et al., 2010. Bayesian filtering of human brain hemodynamic activity elicited by visual short-term maintenance recorded through functional near-infrared spectroscopy (fNIRS). Opt. Express 18 (25), 26550–26568.
Scarpa, F., Brigadoi, S., Cutini, S., et al., 2011. A methodology to improve estimation of stimulus-evoked hemodynamic response from fNIRS measurements. Conf. Proc. IEEE Eng. Med. Biol. Soc. 785–788.
Schecklmann, M., Ehlis, A.C., Plichta, M.M., et al., 2008. Functional near-infrared spectroscopy: a long-term reliable tool for measuring brain activity during verbal fluency. Neuroimage 43 (1), 147–155.
Schelkanova, I., Toronov, V., 2010. Optimal quantitation of the cerebral hemodynamic response in functional near-infrared spectroscopy. Opt. Express 18 (18), 19386–19395.
Schelkanova, I., Toronov, V., 2012. Independent component analysis of broadband near-infrared spectroscopy data acquired on adult human head. Biomed. Opt. Express 3 (1), 64–74.
Scholkmann, F., Spichtig, S., Muehlemann, T., et al., 2010. How to detect and reduce movement artifacts in near-infrared imaging using moving standard deviation and spline interpolation. Physiol. Meas. 31 (5), 649–662.
Scholkmann, F., Gerber, U., Wolf, M., et al., 2013. End-tidal CO_2: an important parameter for a correct interpretation in functional brain studies using speech tasks. Neuroimage 66, 71–79.
Schroeter, M.L., Bücheler, M.M., Müller, K., et al., 2004. Towards a standard analysis for functional near-infrared imaging. Neuroimage 21 (1), 283–290.
Seki, Y., Miyashita, T., Kandori, A., et al., 2012. Simultaneous measurement of neuronal activity and cortical hemodynamics by unshielded magnetoencephalography and near-infrared spectroscopy. J. Biomed. Opt. 17 (10), 107001.
Severinghaus, J.W., 2007. Takuo Aoyagi: discovery of pulse oximetry. Anesth. Analg. 105, S1–S4.
Shimadzu, Japan. www.med.shimadzu.co.jp (Last Visited: 01/30/2013).
Sitaram, R., Zhang, H., Guan, C., et al., 2007. Temporal classification of multichannel near-infrared spectroscopy signals of motor imagery for developing a brain–computer interface. Neuroimage 34 (4), 1416–1427.
Sliney, D.H., 1997. Laser and led eye hazards: safety standards. Opt. Photon. News 8 (9), 31–37.
Soe, N.N., Nakagawa, M., 2008. Chaotic properties of hemodynamic response in functional near infrared spectroscopic measurement of brain activity. Int. J. Biol. Med. Sci. 4 (1), 34–43.
Soellinger, M., Ryf, S., Boesiger, P., et al., 2007. Assessment of human brain motion using cspamm. J. Magn. Reson. Imaging 25 (4), 709–714.
Soellinger, M., Rutz, A.K., Kozerke, S., et al., 2009. 3D cine displacement-encoded MRI of pulsatile brain motion. Magn. Reson. Med. 61 (1), 153–162.
Soraghan, C.J., Ward, T.E., Matthews, F., et al., 2008. Optical safety assessment of a near-infrared brain–computer interface. Proc IEE Irish Signals and Systems Conference, pp. 174–179.
Spectratech, Japan. http://www.spectratech.co.jp/En/indexEn.html (Last Visited: 01/30/2013).
Spichtig, S. Scholkmann, F., Chin, L., 2012. Assessment of intermittent umts electromagnetic field effects on blood circulation in the human auditory region using a near-infrared system. Bioelectromagnetics 33 (1), 40–45.
Srinivasan, S., Pogue, B.W., Carpenter, C., et al., 2007. Developments in quantitative oxygen-saturation imaging of breast tissue in vivo using multispectral near-infrared tomography. Antioxid. Redox Signal. 9 (8), 1143–1156.
Strangman, G., Boas, D.A., Sutton, J.P., 2002. Non-invasive neuroimaging using near-infrared light. Biol. Psychiatry 52 (7), 679–693.
Strangman, G., Franceschini, M.A., Boas, D.A., 2003. Factors affecting the accuracy of near-infrared spectroscopy concentration calculations for focal changes in oxygenation parameters. Neuroimage 18 (4), 865–879.
Strik, C., Klose, U., Erb, M., et al., 2002. Intracranial oscillations of cerebrospinal fluid and blood flows: analysis with magnetic resonance imaging. J. Magn. Reson. Imaging 15 (3), 251–258.
Sulzer, J., Haller, S., Scharnowski, F., et al., 2013. Real-time fMRI neurofeedback: progress and challenges. Neuroimage 76, 386–399.
Suzuki, S., Takasaki, S., Ozaki, T., et al., 1999. A tissue oxygenation monitor using NIR spatially resolved spectroscopy. Proc. SPIE 3597, 582–592.
Szabo, K., Lako, E., Juhasz, T., et al., 2011. Hypocapnia induced vasoconstriction significantly inhibits the neurovascular coupling in humans. J. Neurol. Sci. 309 (1–2), 58–62.
Tachtsidis, I., Elwell, C.E., Lee, C.W., et al., 2003. Spectral characteristics of spontaneous oscillations in cerebral haemodynamics are posture dependent. Adv. Exp. Med. Biol. 540, 31–36.
Tachtsidis, I., Elwell, C.E., Leung, T.S., et al., 2004. Investigation of cerebral haemodynamics by near-infrared spectroscopy in young healthy volunteers reveals posture-dependent spontaneous oscillations. Physiol. Meas. 25 (2), 437–445.
Tachtsidis, I., Leung, T.S., Devoto, L., et al., 2008a. Measurement of frontal lobe functional activation and related systemic effects: a near-infrared spectroscopy investigation. Adv. Exp. Med. Biol. 614, 397–403.
Tachtsidis, I., Leung, T.S., Tahir, B., et al., 2008b. A hybrid multi-distance phase and broadband spatially resolved algorithm for resolving absolute concentrations of chromophores in the near-infrared light spectrum: results from studies in dynamic phantoms. Biomed. Opt. BSuE76.
Tachtsidis, I., Leung, T.S., Tisdall, M.M., et al., 2008c. Investigation of frontal cortex, motor cortex and systemic haemodynamic changes during anagram solving. Adv. Exp. Med. Biol. 614, 21–28.
Tachtsidis, I., Leung, T.S., Chopra, A., et al., 2009. False positives in functional near-infrared topography. Adv. Exp. Med. Biol. 645, 307–314.
Tachtsidis, I., Koh, P.H., Stubbs, C., et al., 2010. Functional optical topography analysis using statistical parametric mapping (spm) methodology with and without physiological confounds. Adv. Exp. Med. Biol. 662, 237–243.
Tachtsidis, I., Tisdall, M.M., Pritchard, C., et al., 2011. Analysis of the changes in the oxidation of brain tissue cytochrome-c-oxidase in traumatic brain injury patients during hypercapnoea: a broadband NIRS study. Adv. Exp. Med. Biol. 701, 9–14.
Tachtsidis, I., Bainbridge, A., Faulkner, S., et al., 2012. In-vivo measurements of brain haemodynamics and energetics using multimodal spectroscopy in perinatal hypoxia–ischaemia. Digital Holography and Three-Dimensional Imaging, p. JM3A.27.
Takahashi, T., Takikawa, Y., Kawagoe, R., et al., 2011. Influence of skin blood flow on near-infrared spectroscopy signals measured on the forehead during a verbal fluency task. Neuroimage 57 (3), 991–1002.
Takahashi, K., Tanaka, T., Hiroyuki, N., et al., 2012. A modeling of cerebral blood flow changes due to head motion for fNIRS. 2012 International Symposium on Optomechatronic Technologies.
Tanaka, H., Katura, T., Sato, H., 2013. Task-related component analysis for functional neuroimaging and application to near-infrared spectroscopy data. Neuroimage 64, 308–327.
Taroni, P., Comelli, D., Pifferi, A., et al., 2007. Absorption of collagen: effects on the estimate of breast composition and related diagnostic implications. J. Biomed. Opt. 12 (1), 014021.
Tax, N., Pichler, G., Grossauer, K., et al., 2011. Tilting the head changes cerebral haemodynamics in neonates. Neonatology 100 (3), 253–259.
TechEn, USA. www.nirsoptix.com (Last Visited: 01/30/2013).
Tian, F.H., Alexandrakis, G., Liu, H.L., 2009. Optimization of probe geometry for diffuse optical brain imaging based on measurement density and distribution. Appl. Opt. 48 (13), 2496–2504.
Tian, F., Niu, H., Khan, B., et al., 2011. Enhanced functional brain imaging by using adaptive filtering and a depth compensation algorithm in diffuse optical tomography. IEEE Trans. Biomed. Eng. 30 (6), 1239–1251.
Tikhonov, A.N., Arsenin, V.Y., 1977. Solution of Ill-posed Problems.Winston & Sons, Washington.
Tinius, T., Pa, T.T., 2005. New Developments in Blood Flow Hemoencephalography. Haworth Press Inc.
Tisdall, M.M., Tachtsidis, I., Leung, T.S., et al., 2007. Near-infrared spectroscopic quantification of changes in the concentration of oxidized cytochrome c oxidase in the healthy human brain during hypoxemia. J. Biomed. Opt. 12 (2), 024002.
TOAST, 2013. Website http://web4.cs.ucl.ac.uk/research/vis/toast/ (Last Visited: 01/30/2013).
Tong, Y., Lindsey, K.P., deB Frederick, B., 2011. Partitioning of physiological noise signals in the brain with concurrent near-infrared spectroscopy and fMRI. J. Cereb. Blood Flow Metab. 31 (12), 2352–2362.
Tong, Y., Hocke, L.M., Nickerson, L.D., et al., 2013. Evaluating the effects of systemic low frequency oscillations measured in the periphery on the independent component analysis results of resting state networks. Neuroimage 76, 202–215.
Toronov, V., Franceschini, M.A., Filiaci, M., et al., 2000. Near-infrared study of fluctuations in cerebral hemodynamics during rest and motor stimulation: temporal analysis and spatial mapping. Med. Phys. 27 (4), 801–815.
Toronov, V., Webb, A., Choi, J.H., et al., 2001. Investigation of human brain hemodynamics by simultaneous near-infrared spectroscopy and functional magnetic resonance imaging. Med. Phys. 28 (4), 521–527.
Trajkovic, I., Reller, C., Wolf, M., et al., 2009. Modelling and filtering almost periodic signals by time-varying Fourier series with application to near-infrared spectroscopy. 17th European, Signal Processing Conference, pp. 632–636.
Trajkovic, I., Scholkmann, F., Wolf, M., 2011. Estimating and validating the interbeat intervals of the heart using near-infrared spectroscopy on the human forehead. J. Biomed. Opt. 16 (8), 087002.
Trajkovic, I., Reller, C., Wolf, M., 2012. Modelling and filtering of physiological oscillations in near-infrared spectroscopy by time-varying Fourier series. Adv. Exp. Med. Biol. 737, 307–313.
Tsuzuki, D., Dan, I., Dan, H., et al., 2012. Adaptive hemodynamic response function to optimize differential temporal information of hemoglobin signals in functional near-infrared spectroscopy. 2012 ICME International Conference on Complex Medical Engineering (CME), pp. 788–792.
UCL, 2005. Specific extinction spectra of tissue chromophores. http://www.medphys.ucl.ac.uk/research/borl/research/NIR_topics/spectra/spectra.htm (Last Visited: 1/7/2013).
Uludağ, K., Steinbrink, J., Kohl-Bareis, M., et al., 2004a. Cytochrome-c-oxidase redox changes during visual stimulation measured by near-infrared spectroscopy cannot be explained by a mere cross talk artefact. Neuroimage 22 (1), 109–119.
Uludağ, K., Steinbrink, J., Villringer, A., et al., 2004b. Separability and cross talk: optimizing dual wavelength combinations for near-infrared spectroscopy of the adult head. Neuroimage 22 (2), 583–589.
University College London, Uk. Optical topography system http://www.ucl.ac.uk/medphys/research/borl/imaging/topography (Last Visited: 01/30/2013).
Vaithianathan, T. Tullis, I.D.C. Everdell, N., 2004. Design of a portable near infrared system for topographic imaging of the brain in babies. Rev. Sci. Instrum. 75 (10), 3276–3283.

van der Sluijs, M.C., Colier, W.N.J.M., Houston, R.J.F., et al., 1998. A new and highly sensitive continuous wave near infrared spectrophotometer with multiple detectors. Photon Propagation in Tissues Iii, Proceedings Of, 3194, pp. 63–72.
van Veen, R.L.P., Sterenborg, H.J.C.M., Pifferi, A., et al., 2004. Determination of VIS-NIR absorption coefficients of mammalian fat, with time- and spatially resolved diffuse reflectance and transmission spectroscopy. Biomedical Topical Meeting, p. SF4.
Villringer, A., Planck, J., Hock, C., et al., 1993. Near infrared spectroscopy (NIRS): a new tool to study hemodynamic changes during activation of brain function in human adults. Neurosci. Lett. 154 (1–2), 101–104.
Virtanen, J., Noponen, T., Meriläinen, P., 2009. Comparison of principal and independent component analysis in removing extracerebral interference from near-infrared spectroscopy signals. J. Biomed. Opt. 14 (5), 054032.
Virtanen, J., Noponen, T., Salmi, T., et al., 2012. Impaired cerebral vasoreactivity may cause cerebral blood volume dip following obstructive sleep apnea termination. Sleep Breath. 16 (2), 309–312.
Vogel, A., Venugopalan, V., 2003. Mechanisms of pulsed laser ablation of biological tissues. Chem. Rev. 103 (2), 577–644.
von Vierordt, K., 1876. Die quantitative Spectralanalyse in ihrer Anwendung auf Physiologie, Physik, Chemie und Technologie. Verlag H. Laupp, Tübingen.
Wahl, M., Schilling, L., 1993. Regulation of cerebral blood flow—a brief review. Acta Neurochir. Suppl. (Wien) 59, 3–10.
Wahr, J.A., Tremper, K.K., Samra, S., et al., 1996. Near-infrared spectroscopy: theory and applications. J. Cardiothorac. Vasc. Anesth. 10 (3), 406–418.
Ward, K.R., Ivatury, R.R., Barbee, R.W., et al., 2006. Near infrared spectroscopy for evaluation of the trauma patient: a technology review. Resuscitation 68 (1), 27–44.
White, B.R., Snyder, A.Z., Cohen, A.L., et al., 2009. Resting-state functional connectivity in the human brain revealed with diffuse optical tomography. Neuroimage 47 (1), 148–156.
Wolf, M., Evans, P., Bucher, H.U., et al., 1997. Measurement of absolute cerebral haemoglobin concentration in adults and neonates. Adv. Exp. Med. Biol. 428, 219–227.
Wolf, M., Wolf, U., Toronov, V., et al., 2002. Different time evolution of oxyhemoglobin and deoxyhemoglobin concentration changes in the visual and motor cortices during functional stimulation: a near-infrared spectroscopy study. Neuroimage 16 (3A), 704–712.
Wolf, M., Ferrari, M., Quaresima, V., 2007. Progress of near-infrared spectroscopy and topography for brain and muscle clinical applications. J. Biomed. Opt. 12 (6), 062104.
Wolf, U., Toronov, V., Choi, J.H., et al., 2011. Correlation of functional and resting state connectivity of cerebral oxy-, deoxy-, and total hemoglobin concentration changes measured by near-infrared spectrophotometry. J. Biomed. Opt. 16 (8), 087013.
Wolf, M., Naulaers, G., van Bel, F., et al., 2012. A review of near infrared spectroscopy for term and preterm newborns. J. Near Infrared Spectrosc. 20 (1), 43–55.
Worsley, K.J., Friston, K.J., 1995. Analysis of fMRI time-series revisited-again. Neuroimage 2 (3), 173–181.
Wyatt, J.S., Cope, M., Delpy, D.T., et al., 1990. Quantitation of cerebral blood volume in human infants by near-infrared spectroscopy. J. Appl. Physiol. 68 (3), 1086–1091.
Xu, H., Springett, R., Dehghani, H., et al., 2005. Magnetic-resonance-imaging-coupled broadband near-infrared tomography system for small animal brain studies. Appl. Opt. 44 (11), 2177–2188.
Yamada, T., Umeyama, S., Matsuda, K., 2009. Multidistance probe arrangement to eliminate artifacts in functional near-infrared spectroscopy. J. Biomed. Opt. 14 (6), 064034.
Yamada, T., Umeyama, S., Matsuda, K., 2010. A multidistance probe arrangement NIRS for detecting absorption changes in cerebral gray matter layer. Multimodal Biomedical Imaging V. Proc. SPIE 7557.
Yamada, T., Umeyama, S., Matsuda, K., 2012. Separation of fNIRS signals into functional and systemic components based on differences in hemodynamic modalities. PLoS One 7 (11), e50271.
Yamamoto, T., Maki, A., Kadoya, T., et al., 2002. Arranging optical fibres for the spatial resolution improvement of topographical images. Phys. Med. Biol. 47 (18), 3429–3440.
Yamashita, Y., Maki, A., Koizumi, H., 2001. Wavelength dependence of the precision of noninvasive optical measurement of oxy-, deoxy-, and total-hemoglobin concentration. Med. Phys. 28 (6), 1108–1114.
Ye, J.C., Tak, S., Jang, K.E., et al., 2009. NIRS-SPM: statistical parametric mapping for near-infrared spectroscopy. Neuroimage 44 (2), 428–447.
Zhang, Q., Brukilacchio, T.J., Gaudett, T., et al., 2001. Experimental comparison of using continuous-wave and frequency-domain diffuse optical imaging systems to detect heterogeneities. Optical Tomography and Spectroscopy of Tissue IV, 2 (7), pp. 219–238.
Zhang, X., Toronov, V.Y., Fabiani, M., et al., 2005a. The study of cerebral hemodynamic and neuronal response to visual stimulation using simultaneous NIR optical tomography and BOLD fMRI in humans. Proc. Soc. Photo Opt. Instrum. Eng. 5686 (115), 566–572.
Zhang, Y., Brooks, D.H., Franceschini, M.A., et al., 2005b. Eigenvector-based spatial filtering for reduction of physiological interference in diffuse optical imaging. J. Biomed. Opt. 10 (1), 11014.
Zhang, Q., Brown, E.N., Strangman, G.E., 2007a. Adaptive filtering for global interference cancellation and real-time recovery of evoked brain activity: a Monte Carlo simulation study. J. Biomed. Opt. 12 (4), 044014.
Zhang, Q., Brown, E.N., Strangman, G.E., 2007b. Adaptive filtering to reduce global interference in evoked brain activity detection: a human subject case study. J. Biomed. Opt. 12 (6), 064009.
Zhang, Q., Strangman, G.E., Ganis, G., 2009. Adaptive filtering to reduce global interference in non-invasive NIRS measures of brain activation: how well and when does it work? Neuroimage 45 (3), 788–794.
Zhang, H., Zhang, Y.J., Lu, C.M., et al., 2010a. Functional connectivity as revealed by independent component analysis of resting-state fNIRS measurements. Neuroimage 51 (3), 1150–1161.
Zhang, Y., Sun, J., Rolfe, P., 2010b. Monte carlo study for physiological interference reduction in near-infrared spectroscopy based on empirical mode decomposition. J. Mod. Opt. 57 (21), 2159–2169.
Zhang, H., Duan, L., Zhang, Y.J., et al., 2011a. Test–retest assessment of independent component analysis-derived resting-state functional connectivity based on functional near-infrared spectroscopy. Neuroimage 55 (2), 607–615.
Zhang, Q., Yan, X., Strangman, G.E., 2011b. Development of motion resistant instrumentation for ambulatory near-infrared spectroscopy. J. Biomed. Opt. 16 (8), 087008.
Zhang, Y., Sun, J., Rolfe, P., 2011c. Reduction of global interference in functional multidistance near-infrared spectroscopy using empirical mode decomposition and recursive least squares: a Monte Carlo study. J. Eur. Opt. Soc. Rapid Publ. 6, 11033.
Zhang, X., Niu, H., Song, Y., et al., 2012a. Activation detection in fNIRS by wavelet coherence. Medical Imaging 2012: Biomedical Applications in Molecular, Structural, and Functional Imaging. Proc. SPIE 8317, 831712.
Zhang, Y., Sun, J.W., Rolfe, P., 2012b. RLS adaptive filtering for physiological interference reduction in NIRS brain activity measurement: a Monte Carlo study. Physiol. Meas. 33 (6), 925–945.
Zhu, T., Faulkner, S., Madaan, T., et al., 2012. Optimal wavelength combinations for resolving in-vivo changes of haemoglobin and cytochrome-c-oxidase concentrations with NIRS. Biomed. Opt. JM3A.6.
Zijlstra, W.G., Buursma, A., Van Assendelft, O.W., 2000. Visible and Near Infrared Absorption Spectra of Human and Animal Haemoglobin: Determination and Application.CRC Press, Zeist, The Netherlands.
Zimmermann, R., Braun, F., Achtnich, T., et al., 2013a. Silicon photomultipliers for improved detection of low light levels in miniature near-infrared spectroscopy instruments. Biomed. Opt. Express 659–666.
Zimmermann, R., Marchal-Crespo, L., Edelmann, J., et al., 2013b. Detection of motor execution using a hybrid fNIRS-biosignal BCI: a feasibility study. J. Neuroeng. Rehabil. 10 (4).
Zysset, C., Nasseri, N., Buthe, L., et al., 2013. Textile integrated sensors and actuators for near-infrared spectroscopy. Opt. Express 21 (3), 3213–3224.